



# FINAL PUBLISHABLE JRP REPORT

JRP-Contract number	IND51	
JRP short name	MORSE	
JRP full title	Metrology for optical and RF communication systems	
Version numbers of latest contracted Annex Ia and Annex Ib against which the assessment will be made	Annex Ia:	V1.1
	Annex Ib:	V1.0
Period covered (dates)	From 1 July 2013	To 30 June 2016
JRP-Coordinator		
Name, title, organisation	Dr David Humphreys, Principal Research Scientist, NPL, UK	
Tel:	+44 208 943 6389	
Email:	david.humphreys@npl.co.uk	
JRP website address	<a href="http://www.emrp-ind51-morse.org">www.emrp-ind51-morse.org</a>	
Other JRP-Partners		
Short name, country	NPL, United Kingdom CMI, Czech Republic LNE, France METAS, Switzerland PTB, Germany Keysight DE, Germany Dassault, France	
REG1-Researcher (associated Home Organisation)	Dr. Marco Spirito TU Delft, Netherlands	Start date: 1 July 2013 Duration: 36 months
REG2-Researcher (associated Home Organisation)	Dr. Laurent Le Coq UR1, France	Start date: 1 July 2013 Duration: 36 months
REG3-Researcher (associated Home Organisation)	Prof. Peter Andrekson, Chalmers, Sweden	Start date: 1 Nov 2013 Duration: 18 months

**Report Status: PU Public**



## TABLE OF CONTENTS

1	Executive Summary .....	3
2	Project context, rationale and objectives .....	5
2.1	Context .....	5
2.2	Rationale .....	5
2.2.1	Specific needs .....	6
2.3	Objectives .....	6
3	Research results .....	8
3.1	Terrestrial wireless communication .....	8
3.1.1	Over-the-air measurement of Multiple-Input Multiple-Output RF communication .....	8
3.1.2	Power measurement for Over-the-air Multiple In-Multiple-Out (OTA-MIMO) systems .....	10
3.1.3	Efficient measurement of Smart, adaptive reconfigurable and wearable antennas .....	11
3.2	Efficient Antenna Measurement .....	13
3.2.1	Assessment of existing antenna test methods combining modelling and measurement .....	13
3.2.2	Improved antenna test methods using combined measurement and modelling .....	15
3.2.3	Improved antenna test method using compact antenna test range (CATR) .....	18
3.2.4	Low-reflectivity field sampling using an optoelectronic probe .....	20
3.2.5	Measurement of antennas over a controllable temperature range .....	22
3.3	Optical Communications .....	23
3.3.1	Characterisation of photoreceiver systems .....	23
3.3.2	Characterisation of high-speed transmitters for advanced optical modulation formats using coherent detection .....	28
3.4	Key scientific results .....	32
4	Actual and potential impact .....	33
4.1	Direct impact activities undertaken .....	33
4.1.1	Advisory Board .....	33
4.1.2	Newsletters .....	33
4.1.3	Conference presentations .....	34
4.1.4	Journal publications .....	34
4.1.5	Best practice guides and other protocols and procedures .....	34
4.1.6	Trade journals and popular press .....	35
4.1.7	Input to standardisation .....	35
4.1.8	Workshops .....	35
4.1.9	Training and dissemination .....	36
4.1.10	Exploitation .....	37
4.2	Actual and Potential impact .....	38
4.3	Early uptake .....	38
4.4	Wider and long-term impacts .....	38
5	Website address and contact details .....	38
6	List of publications .....	41

## 1 Executive Summary

### Introduction

Society relies on reliable and efficient data communications; the sending of data through the air and point to point. However there are many interdependent technologies that are needed to ensure reliability and efficiency, ultimately providing a seamless experience for the user. This project developed a traceable measurement infrastructure and modelling techniques for mobile, satellite and optical communications to minimise the time needed to test and improve new devices, and therefore reduce time to market. Traceable measurement of signal and power output from devices ensures conformity to standards and safeguards end users. New measurement techniques for rapid characterisation of optical components allows industry to monitor device performance.

### The Problem

Traffic on telecommunication networks is currently growing by around 40 % each year, which will soon lead to a capacity crunch unless new technologies are introduced to maintain quality and prevent disruption to the networks on which the modern world relies. This project will support the work of the European Telecommunications Standards Institute (ETSI) and the International Electrotechnical Commission (IEC), and will result in new measurement procedures and services to support the introduction of new multiple antenna systems, satellite system testing and the next generation of optical communications equipment. It aims to help instrument, component and satellite manufacturers to develop and implement new systems, minimise test and measurement costs and reduce the time to market for new products and services.

Technologies such as reconfigurable and multiple antennas can increase the capacity and quality of wireless communications, however they also make testing more complex and time consuming. When building a satellite, antenna testing happens during a high-risk stage of development, therefore more complicated antennas could potentially disrupt the satellite companies' tight delivery schedules. State-of-the-art satellites can simultaneously create multiple transmission beams that cover different areas on the earth's surface and this increased complexity extends the test duration and makes it more complex. Reliable and robust methods to cut the test-time are needed to maintain the tight delivery-schedules. During the development of each next-generation system general-purpose test equipment is needed to determine the performance. Good metrology that extends the capability of this test-equipment will help the research, and improve service quality.

No single National Measurement Institute can address all of these challenges and so the project consortium includes several universities that have major test-bed facilities, as well as industry through component and test-equipment manufacturers.

### The Solution

The key project objective was to provide traceable measurement support in three key areas: Terrestrial mobile communications; efficient antenna measurement, primarily to support the satellite industry; and core optical communications systems which carry >100 Gb/s in a single channel and use communication formats drawn from RF but at a much higher data-rate. In all these areas there are many measurement challenges because the systems and their supporting test equipment development occur simultaneously.

### Impact

Future telecommunications growth depends on the development and delivery of new technology. This project developed the underlying metrology for both research and deployment activities, and advanced the test facilities to enable industry and research to provide a competitive edge within Europe. In addition, it generated a first-hand appreciation within the NMIs and universities of the measurement issues. An advisory board comprising members from ESA, ETSI, Keysight, Finisar and NEC has ensured good industrial focus throughout the project.

This project developed traceable measurement infrastructure and modelling techniques for mobile, satellite and optical communications to minimise the time it takes to test and improve new devices, and therefore reduce time to market. Traceable measurement for signal and power output from devices ensures conformity to standards and safeguards end users. New measurement techniques for rapid characterisation of optical components allows industry to monitor device performance.

Several of the project outputs were focussed to provide industrial impact through state-of-the-art facilities and calibration capability or services. Examples include:

- World first traceable RF field calibration for fourth generation (4G) systems known as LTE (long-term-evolution) to qualify health and exposure limits for non-ionizing radiation and protect EU citizens and workers.
- A traceably calibrated and upgraded Compact Antenna Range facility for mm-wave operation. This system includes software correction of mechanical errors and is available for academic and industrial research.
- Extension of fast electrical waveform >100 GHz facilities for single and dual photodiode calibration, required for >100 Gb/s optical communication components and systems.

In addition to 19 conference presentations, seven full papers were published in leading journals. Two full-day workshops allowed the scientists to interact directly with industry. There were around 30 further publications, including best-practice guides, newsletters, workshop presentations and trade journals. This material is available electronically through the project website, the NPL website and the Euramet repository in addition to widely used sources such as Linked-In and personal ResearchGate accounts.

## 2 Project context, rationale and objectives

### 2.1 Context

High quality satellite, fibre and mobile communications are an essential part of modern life and vital to European Industry, with increasing demand for telecommunications growing at 40 % p.a [Error! Bookmark not defined.]. The EU “2020 Digital Agenda for Europe” acknowledges this and set ambitious targets that would have an impact on all areas of the communication network. Industries are addressing this challenge through unlocking the latent capacity of ground-based and satellite-based systems. However, the potential technologies are complex and reliable measurement is required to develop and test innovative solutions in appropriate timescales and costs.

This project ran in parallel with the EU Research and Innovation funding programme “FP7” and “EU Horizon 2020” Framework projects that prioritise ICT research [Error! Bookmark not defined.]. The Europe Commission had previously identified, the need for a well-developed communication infrastructure to promote growth [1], “Digital Infrastructures – both physical and service based – that are key enablers for the smart growth which Europe must achieve in the coming ten years in order to ensure its ability to compete internationally and to generate wealth for its citizens”. This drives the 2020 Digital Agenda for Europe, “Connecting Europe Facility” and “EU Horizon 2020”.

### 2.2 Rationale

The EU “2020 Digital Agenda for Europe” acknowledges the link between good communications infrastructure and wealth creation by the EU citizens and sets ambitious targets that will have an impact on all areas of the communication network. Industries are addressing this challenge through unlocking the latent capacity of ground-based and satellite-based systems. However, the potential technologies are complex and reliable measurement is required to develop and test the next generation of innovative solutions with an appropriate timescale and costs. This project required a team drawn from several NMIs and industry because no individual partner had the breadth of facilities or experience to support all aspects of this research.

The telecommunications industry is global and impacts on a continental scale. The definition of the individual systems and the essential algorithms to make them work are driven through standards bodies that are in turn underpinned by measurement. One of the longer-term goals is to align and collaborate with one or more standards bodies to provide measurement knowledge to support the standards development.

The development and release of new telecommunications systems has several distinct phases. During the initial research phase much of the supporting work is done by simulation, rather than by physical measurement, and is undertaken within universities. Once the basic concepts are in place, for example the use of multiple input, multiple output (MIMO) transmission has been applied in the 4<sup>th</sup> generation mobile communication system (Long-Term Evolution or LTE) but this concept is being greatly developed in the 5<sup>th</sup> generation systems (5G) to increase spatial diversity, initial experimental work is carried out to explore issues that are not captured by simulation and then taken forward to hardware development and standards bodies. In this phase there may not be dedicated test equipment available and only general test equipment is available. This project addresses the measurement issues in MIMO testing and high-speed optical testing that arise from using generalised test equipment at the extremes of its capability. At the end of this process, agreed standards, sufficient to allow manufacture and roll-out of dedicated test equipment will be available, and some test trials will have been performed. In the final phase is roll-out and manufacture. At this point the test equipment and manufacturing are refined and the emphasis changes to making a reliable product at low cost. There will be further development and introduction of new features over the next few years but the overall direction is set.

As communications is a large business it is important to maximise the benefit from the available expertise by focussing on particular metrology aspects of communication technology. In this project our aim was to provide underpinning metrology for mobile communication, optical and satellite communication parts of the network, specifically targeting red-flag areas: Over-The-Air MIMO testing, which still has unresolved standards problems; support for time limited satellite testing through the use of undersampling and finally high-speed optical communication where the test equipment is used to the limits of its capability. By taking this approach we provide some support for all aspects from the network-edge to the network-core. This will aid instrument, component and satellite manufacturers to develop and implement new systems, minimising test and measurement costs and reducing the time to market for new products and services. As a consequence, research outputs such as publications, test facilities and reliable test methods provide a benefit to industry and the research community.

### 2.2.1 Specific needs

Over-The-Air testing of MIMO and other advanced antenna systems presents significant metrology challenges and this has been reflected through a number of European Cooperation on Science and Technology (COST) programmes which facilitate academic knowledge transfer. Measurement of MIMO power is important because a 1 dB loss of sensitivity of the user equipment (UE) corresponds to a 14 % reduction in the effective cell size, which has implications for quality of service, planning and operational costs [2]. At the start of this project no European NMIs were suitably equipped to support industry in this area.

Large satellite communication systems have typical turnaround times of 24 months with costs in the range 400 M€ - 650 M€. Test and validation times are critical and occur at a high-cost stage in the programme cycle. State-of-the-art satellites can simultaneously create multiple transmission beams that cover different areas on the earth's surface and this increased complexity extends the test duration. Reliable and robust methods to cut the test-time by a factor of two or more are needed to maintain the tight delivery-schedules.

The project structure reflects this philosophy and is divided into three distinct technical task areas concentrating on RF terrestrial and mobile communications, efficient antenna measurement strategies and support for high-bandwidth optical communications.

## 2.3 *Objectives*

The project addressed the following scientific and technical objectives;

### 2.3.1.1 **Terrestrial wireless communication**

- Develop Traceable RF power measurement for Over-the-air (OTA) Multiple In-Multiple-Out (MIMO) systems and directly benefit the European communication workers who may be exposed to these RF fields.
- Develop and verify a sound methodology that qualifies the measurement and associated uncertainties for OTA testing of MIMO and adaptive antenna systems.
- Develop accurate, efficient and cost-effective metrological solutions for Smart, adaptive reconfigurable and wearable antennas. Establish with quantified uncertainties the rapid measurement of pattern, gain and efficiency in anechoic environments, and total radiated power/gain diversity in multi-path environments.

### 2.3.1.2 **Sub-Nyquist sampling and EM modelling for efficient antenna measurement**

- Develop and validate a sound methodology that links antenna modelling, sub-Nyquist spatial sampling measurement-strategies with Electromagnetic-Modelling (EM) based interpolation to give a quantified uncertainty for the result. Validate the methods against traditional technique using both small and large antenna structures. Provide a rule-based approach that relates the measurement throughput improvement to the degradation of the uncertainty, allowing an optimum solution.
- Develop an Optoelectronic Low-reflectivity Field-Sampling Probe for operation at 60 GHz.
- Improve the efficiency of Compact Antenna Test Range (CATR) by reducing the number of measurements needed to achieve the required uncertainty. The RF field variations in the measurement region "quiet zone" will be predicted and verified for 60 GHz operation using a scanning system and the Optoelectronic Low-reflectivity Field-Sampling Probe.
- Develop and validate a sound methodology for the testing of antennas over a range of temperatures.

### 2.3.1.3 **Optical Communications**

- Develop traceable characterisation of the vector frequency response of a single photodiode over the range of approximately 1 GHz to >100 GHz complete with an uncertainty budget.
- Develop traceable techniques to characterise differential photodiode pairs that form the core of a coherent receiver system. The common-mode and differential-mode vector frequency responses and

uncertainty budgets are required over the range <1 GHz to >50 GHz, complete with uncertainty budgets.

- Develop measurement and analysis techniques for high spectral-efficiency modulation strategies such as QAM, traceable to electrical-waveform standard primary standards, to underpin the optical test instrumentation and commercial portable secondary reference standards required for terabit coherent optical transport. The technique must provide uncertainties for key parametric measures, such as Error-Vector-Magnitude (EVM).

### 3 Research results

#### 3.1 Terrestrial wireless communication

Measurement of the air interface is important for communication systems and also for the sensor networks that will make up the Internet of Things. National Measurement Institutes have excellent knowledge and facilities to characterise antennas and antenna systems and are familiar with the sources of error. Digital mobile systems were previously tested by direct connection but obtaining reliable and consistent results when testing over-the-air has proved to be difficult. The use of Multiple-Input Multiple-Output (MIMO) antennas, coupled with modulation formats, such as Orthogonal Frequency Division Multiple Access (OFDMA) provides both increased channel capacity and protection against multi-path fading. These two technologies have been embedded in the fourth generation wireless communication systems (4G) such as 3GPP Long-Term-Evolution (LTE). Developing robust test methods has been studied under EC COST Actions 2100 and IC1004. In order to support these systems, it is important to have sound traceability route and to have methods to traceably assess the exposure of EU Citizens to non-ionising radiation. We aimed in this research to provide impact on safety, energy efficiency and the cost of testing in three areas:

1. Develop an understanding of MIMO and measurement systems within European NMIs to support industry's current needs and to be able to provide an underpinning contribution to 5G research.
2. Develop traceable RF power metrology for 4G LTE systems so that the RF field-strengths can be calculated to provide a safe working environment for EU citizens and workers. The impact will be enhanced if the conceptual techniques can be applied to subsequent generations of mobile communication system.
3. Test algorithms for directable antennas that provide energy saving and are important for anticipated future system deployments in IoT, 5G and inter-vehicle communication and sensing.

The Advisory Board facilitated NPL's membership of two relevant CTIA working groups: OTA (Over the air testing) and MUSG, the associated uncertainty subgroup, to improve our understanding of the issues and how to achieve impact from this research.

##### 3.1.1 Over-the-air measurement of Multiple-Input Multiple-Output RF communication

The goal of this objective was to provide a better understanding of the testing of MIMO and smart antennas for mobile communication applications by developing and verifying a sound methodology that qualifies the measurement and associated uncertainties for OTA testing of MIMO and adaptive antenna systems.

##### 3.1.1.1 Overview of the research importance

Systems which transmit a high data-rate signal from a source to a receiver via MIMO channels can be tested using cable links for connecting the channels to give optimal transmission. However the requirement on validating the performance of the system using air links has posed significant metrological challenges to establish cable-like connections between MIMO arrays over the air to ensure maximum data throughput for network infrastructure testing. It is envisaged that this will result in a degraded transmission compared to the cable-link case, due to the following three factors: errors in transmission inherent to each direct antenna link, errors in transmission due to crosstalk on each channel from the opposite antenna, errors due to incorrect setup of the antennas and due to possible environmental factors, for example, an environment that has few multi-path reflections may show a lack of diversity and so the channels cannot be separated.

The work is important because in order to support industry the NMIs must have sufficient understanding of the measurement issues to provide the correct underpinning metrology for future communication systems. Without this understanding they cannot contribute to defining a suitable air-link validation procedure. To gain this knowledge it is vital that facilities exist within the NMIs and their performance is explored and they are accessible to industry.

In operation, the key issue for the communication system is data throughput, which will depend on the environment and other factors. Antenna measurement is well understood but there are unknown issues to providing a robust and reproducible digital measurement of MIMO systems.

##### 3.1.1.2 OTA MIMO measurements beyond the state of the art

There are standards presenting different methods for the OTA characterisation of MIMO antennas. However these methods are complex, require an important infrastructure, and are quite time consuming. Moreover,

there is no real metrological approach in these standards: the testing procedure is so complex in terms of equipment and procedures, that the reproducibility of the results is not guaranteed. Some NMI's have excellent facilities for antenna measurement but little experience of the digital OTA data communication. Although significantly larger MIMO facilities are available in industry these systems can be used with high quality reverberation and anechoic chambers and direct access to traceable RF power standards making the facility extend the state of the art

Within this research, MIMO OTA test facilities for 2 x 2, complete with an air-interface simulation have been set up at NPL and METAS. Also, within the NPL facility there is a unique capability to add a movable interference signal that is out of the reference plane.

### 3.1.1.3 Summary of findings

#### 3.1.1.3.1 Critical review

Characterisation of multiple-input and multiple output (MIMO) antennas (a system that uses multiple antennas and multiple RF paths to improve the channel capacity) is a challenging task. It is necessary to include both antenna and propagation characteristics at the same time when testing MIMO systems.

First a critical overview of existing methods has been performed (literature analysis). The two-stage method has been chosen to perform the characterisation in an efficient way using a real-time signal processing software-defined-radio (SDR) platform. With the two-stage method, the antenna angular sensitivity is first measured in terms of complex transmission coefficients and then this is combined with a channel-model to emulate a real-world environment.

Two test approaches were evaluated experimentally: In the first variant, data gathered experimental from a physical environment has been used for the channel model emulation and in the second variant, the channel model emulation has been derived from a mathematical model, taking into account the specificity of precoding to the MIMO antennas. The ability to simulate the channel emulation requires of course a validated model, but on the other hand, it decreases significantly the complexity and the testing time.

#### 3.1.1.3.2 New facilities

A DSP-focused FPGA-based hardware platform based on NI's PXIe-5644R instruments was developed at NPL. Parts of the system could also be configured as an RF channel emulator to achieve real-time emulation of realistic and complicated environments. A base station emulator, (eNodeB) and user equipment (UE) emulator were built using LabVIEW and C# on this platform (Figure 1). This test platform offers a degree of flexibility over user-programmable channel-model and is envisage to have advantages over fast prototyping, accommodating multiple communications protocols without the need to deploy new hardware.

At METAS, an approach for calculating channel capacity of an MIMO antenna system was developed. By using different precoding methods and measuring channel matrix, the maximum channel capacity of an MIMO

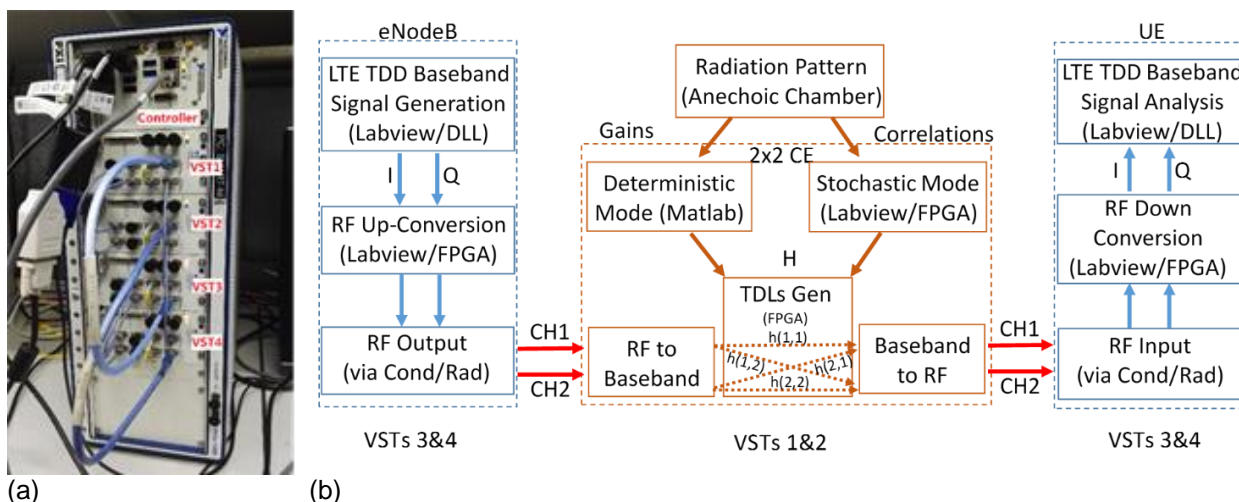


Figure 1 NPL's compact MIMO OTA test system (a) architecture and signal flow (b).

antenna over azimuth angle can be achieved. Thus by comparing the maximum channel capacity, one can judge performance of different MIMO antenna. The results obtained using the two different approaches developed at NPL and METAS to assess performance of MIMO antennas were compared. Polarisation diversity was used as the transmission scheme for this comparison.

**3.1.1.3.3 Test method comparison**

2 x 2 MIMO antennas were measured and their results compared at NPL and METAS to determine the channel matrix for each system. Figure 2 shows the test setup at METAS. Tests at NPL showed good agreement between results at 1.7 GHz and 2.2 GHz. Differences between the measurements at NPL and METAS are due to a slight misalignment between the transmitting and the receiving antennas.

Further measurements to determine the performance in terms of data throughput proved to be a more difficult challenge. A theoretical calculation of MIMO throughput, developed at METAS, was compared with the experimental results measured with the software-radio defined test platform developed at NPL (Figure 1). The throughput performance for different turntable position and total power levels are shown in Figure 3. The throughput scale does not agree very well for the two different approaches suggesting that there remain test issues associated with digital throughput testing (see Figure 3).

**3.1.1.4 Collaboration between partners**

This workpackage required significant collaboration between METAS, NPL and the collaborator WiCO. NPL and METAS share the simulation and experimental and had comparisons between the experimental and the simulation results. The most important problem was the complexity of the task, as well as the complexity of the experimental setup. There was good collaboration over the measurement work, software from METAS and through technical discussions.

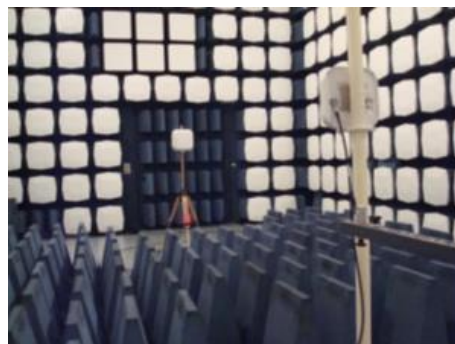


Figure 2 Measurement environment at METAS

**3.1.2 Power measurement for Over-the-air Multiple In-Multiple-Out (OTA-MIMO) systems.**

**3.1.2.1 Overview of the research importance**

The development of a traceable standard for the measurement of MIMO radiation from mobile base stations is an important tool to measure the exposure in terms of electromagnetic radiation that may be attributed to a wireless transmission system, and thus to reliably predict the exposure at maximum data rate. It is a key issue in the protection against non-ionising radiation for workers and EU citizens.

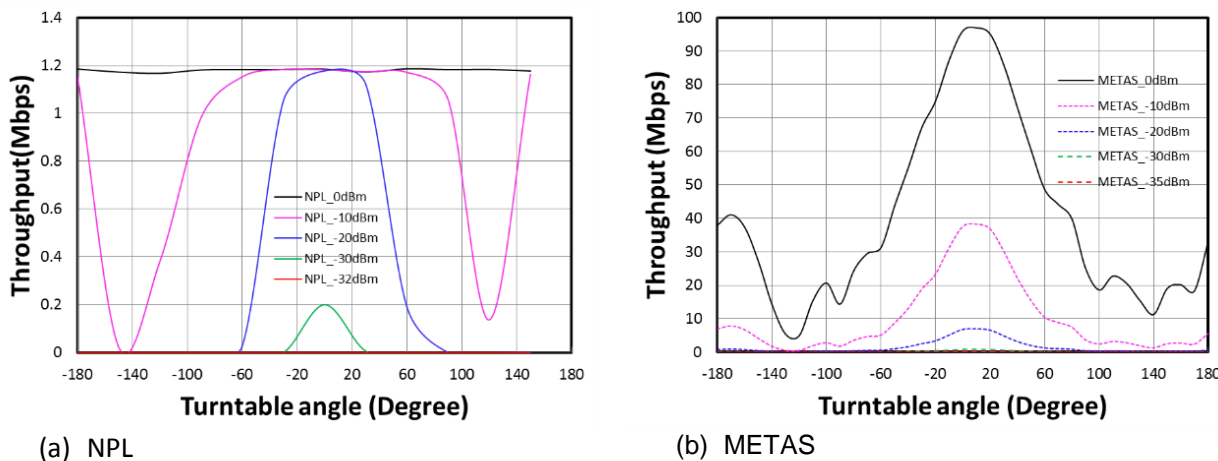


Figure 3 Throughput measured at NPL and METAS for a range of RF powers and turntable positions

Moreover, it is the first step of metrology in digital communication protocols that aims to provide new tools for the estimations of the SNR, for the design of RF front end circuits.

### 3.1.2.2 OTA MIMO power measurements beyond the state of the art

Metrology for digital signal is mainly focussed first on the power metrology in terms of the RMS power, secondly on the metrology of EVM (error vector magnitude). However, this metrology is not able to measure the power of one particular signal within an OFDM modulated signal that can be attributed to one of the MIMO antennas. Commercial devices (e.g. Narda Field-probes) are available on the market that claim to measure these signals, but unfortunately, the measurement systems cannot be calibrated. It was therefore essential to develop an experimental setup and techniques in order to allow the calibration of these devices.

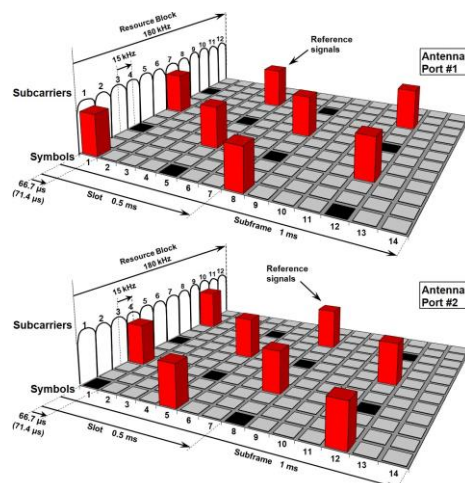
### 3.1.2.3 Summary of findings

We used the LTE protocol, the current generation of mobile communication systems, as the prototype modulated signal. Within this project we have realised, a system with analysis software to measure LTE signals in order to determine the power of LTE reference signals  $RS_0$  and  $RS_1$  (see Figure 4 from [3]) in a way that it is traceable to the International System of Unit (SI). Conducted experiments have shown that the uncertainty of the LTE reference signal measurements is of 0.05 dB ( $k=2$ ). Moreover, the robustness of the power measurements has been demonstrated with a fading simulator.

This calibration capability, believed to be a world first, is now available at METAS and the first calibration certificates for LTE receivers have been issued.

### 3.1.2.4 Collaboration between partners

METAS performed all key elements of this work and collaborated with NPL and LNE to discuss and verify the approach. There was also an interaction with ETH which led to the serendipitous development of a new modulation format.



### 3.1.3 Efficient measurement of Smart, adaptive reconfigurable and wearable antennas

The main objective of this work was to develop suitable algorithms to characterise configurable smart antennas without having to exercise all states.

#### 3.1.3.1 Overview of the research importance

Modern communication systems in telecom and mm-wave bands make extensive use of complex antenna arrays front-end to increase the transmitter (Tx) and the receiver (Rx) antenna gain, to increase the link power budget. Such systems require pre-characterisation of the antenna array settings in order to relate the electronics setting/states to the radiation pattern main beam direction. Such measurements can be extremely time consuming due to the large number of antennas and states permitted in the array. Integrated mm-wave systems require broad-band transitions in close proximity to the antenna/antenna array. Such transitions can

Figure 4 Downlink Cell-Specific Reference signal (normal cyclic prefix) for two antenna ports. Sequences are mapped on the resource element with red colored blocks and black resource elements are set to zero.

partially radiate, perturbing the radiation pattern of the complete system when compared to stand alone antenna/antenna array structures.

### 3.1.3.2 Smart antenna measurements beyond the state of the art

There are many “smart antenna”, adaptive and dynamically reconfigurable antenna systems in use or being considered, where the antenna radiation pattern can be altered to enhance radio link performance, reduce the impact of interference signals and reduce the power requirements. However, these pose metrological challenges as the antennas are small and may have many operating modes which must be characterised. Although these are an emergent technology, their adoption by industry is hampered by cost issues and lack of accurate and cost effective metrology to characterise their performance. Hence it is important to develop metrology for rapid and cost effective measurement of smart adaptive antennas to bring about step change in the application of emergent antenna technologies to wireless networks. The idea of this characterisation of the smart antennas is to perform Signal to Interference Ratio (SIR) measurements in a very efficient way, as well as to quantify uncertainties.

### 3.1.3.3 Summary of findings

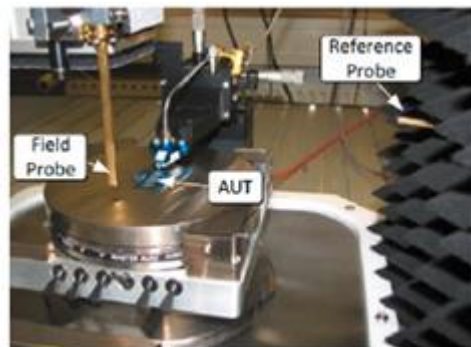
We addressed two different adaptive beamforming antenna measurements approaches to cover mm-wave and low-frequency (<6 GHz) systems.

#### 3.1.3.3.1 First approach – mm-wave

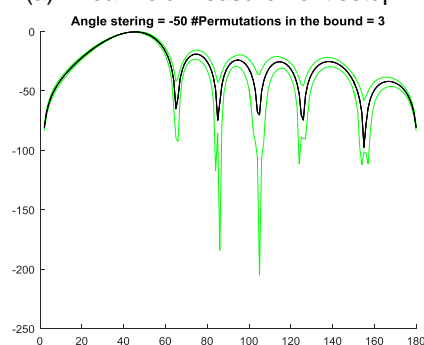
In the first approach, we have developed and evaluated a millimetre-wave planar near-field system to characterise antennas operating in the 60 GHz and 94 GHz band (see Figure 5). To reduce the measurement time for phased-array receivers we have developed a quick method to determine the compliance to specification that reduces the measurement time of the phased-array receiver front-end. The software can find the projected error bounds to the nominal pattern for a given fabrication error (i.e., mapped as a phase/delay mismatch). The software takes into account the maximum allowed phase-error for each array-element in order to determine a pass/fail pattern.

#### 3.1.3.3.2 Second approach – low frequency (< 6 GHz)

In the second approach, we have developed an adaptive beamforming code using simultaneous perturbation stochastic approximation (SPSA) algorithm where the maximum cross-correlation coefficient (MCCC) algorithm (that provides the optimum weight during each SPSA iteration so to enable beamforming) is implemented. A series of smart antenna radiated measurements have been performed with the developed SPSA/MCCC adaptive beamforming algorithm.



(a) Near-field measurement setup



(b) Measurement results

Figure 5 (a) shows the proposed measurement setup for system embedded antennas at mm-wave frequencies, and (b) shows the results for bound for a four element linear antenna array with maximum allowed error of  $\pm 5$  degrees at the antenna

The experimental layout and measured results are shown in *Figure 6* for a 12-element electronically steerable parasitic array radiator (ESPAR) smart antenna [4]. An interesting point noted was that the algorithm often found similar but different solution, suggesting the presence of local minima or to a slight change to the environment [5].

### 3.1.3.4 Collaboration between partners

This was a good collaboration between three partners: TU-Delft, NPL, and METAS. The main work was realised between NPL and TU-Delft. METAS was the leading the work package and responsible for a critical review of the work.

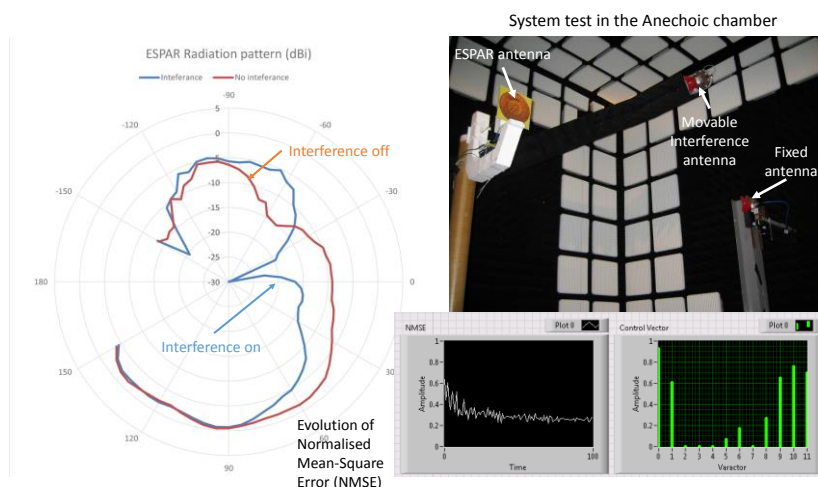


Figure 6 Measured Smart antenna adaptive beamforming for a 12-element parasitic array antenna using the real-time FPGA software defined platform facilities to adapt the antenna pattern to suppress an interference signal. The evolution of the Normalized Mean-Square Error shows the improvement.

## 3.2 Efficient Antenna Measurement

Antenna systems are becoming more complicated, with integrated signal processing allowing multi-beam management. They are also often integrated into large structures, such as satellite payloads. Two general approaches are being employed to cope with the testing challenges of these systems; the first is the design of efficient near-field sampling algorithms and the second is the use of high accuracy far-field systems like Compact ranges which give direct access to the far-field gain of antennas.

This theme within the project has both a general and a specific focus. The general problem is that the antenna assemblies, such as satellites and multi-antenna terrestrial sites, are becoming increasingly complex and this impacts the cost of testing and commissioning. The specific tasks are focussed to deliver particular industry needs, such as the qualification of antennas over a range of temperatures or providing software corrections to achieve an improved performance for a major antenna facility.

### 3.2.1 Assessment of existing antenna test methods combining modelling and measurement

The objective was to determine a baseline for the current state-of-the-art and provide an overview of existing methods used to measure or to predict the RF field from antennas in free space. The study includes the methods used to combine measurements and prediction as this is relevant to develop and verify the achievable performance accuracy of undersampling methods. A critical assessment of the techniques was made to determine their validity.

#### 3.2.1.1 Overview of the research importance

It is essential to provide a baseline data set along with adequate tools to enable the research. We anticipated that there will be the errors associated with near-field or far-field antenna measurement. In order to quantify the errors associated with near-field or far-field antenna measurements, it is essential to have confidence in the mathematical algorithms used to convert the results from one geometry to another.

#### 3.2.1.2 Extending the state of the art

The studies captured the state of the art to provide a baseline. It is important to capture both the positive results and determine the limitations of extrapolation and prediction. The validated transform software extends the state of the art.

#### 3.2.1.3 Summary of findings

The results are summarised as four reports and a supporting data set, covering the available software and its suitability and limitations, a critical review of the existing work on undersampling techniques.

### 3.2.1.3.1 Antenna Software Modelling Packages

A critical review of a number of Antenna Software Modelling Packages has been performed and the results are summarised as a report [6]. The findings suggest that IDS ADF-EMS and Feko's software packages were considered the most promising candidates for the antenna-modelling in this project as they can deal with large structures.

### 3.2.1.3.2 Under-sampling strategies for antenna pattern measurement

Under-sampling is a compressed sensing method that uses prior knowledge to minimise the required measured data needed. If the spatial frequency content of the difference data between the measured data and the prior knowledge data is less than that of the measured data, then the measured data can be sampled below the Nyquist rate.

We have compared several under-sampling strategies, and performed an analysis of algorithms used on previous measured data. The results are summarised in a report [7], which also includes a comprehensive list of publications.

Also, if the antenna pattern can be described by a limited number of basis-functions [8], such as the element patterns in an array antenna, then the number of acquired data points can be reduced to the number of basis-functions used.

Two interpolation schemes studied were kriging [9], and the Papoulis-Gerchberg Method [10-11]. These were not found to be of general use in Antenna Measurements.

### 3.2.1.3.3 Transform and antenna measurement strategies

This work compared the measurement speed of a selection of different advanced antenna test methods against a set of experimental conditions (antenna size, directivity, frequency) for spherical, far-field and planar sampling based as shown in Figure 7.

The planar range can measure a unit under test in a stationary position and is the most suitable for testing satellite payloads. Spherical ranges are the most promising for testing broad beam antennas, such as base station antennas, and are of equivalent speed providing the range length to antenna diameter ratio is greater than 3.5.

Compact ranges suffer from coupling between the feed and the test item, especially if the test item has a lot of metal surfaces.

The equivalent source methods are very promising in the reduction of truncation errors [12]. These methods are still in their early stages. However truncated and thinned measurement schemes have the potential to reduce measurement times by a factor of 6 to 9 times. Methods are also available to use non-equispaced measurement grids [13], [14] and [15].

### 3.2.1.3.4 CATR test models and coupling between the quiet-zone field and the source

A summary of the different Compact Antenna Test-Range (CATR) designs and their positioning systems has been prepared [16] and the factors limiting the performance of a CATR, are edge diffraction, internal coupling, imperfect reflector geometry (see Figure 8) and multipath effects in the surrounding anechoic chamber.

Electromagnetic Modelling of CATRs using full wave methods is limited at high frequencies due to their large electrical size. High frequency techniques, such as Physical Optics (PO) and Geometrical Optics (GO) are generally used combined with full wave techniques to

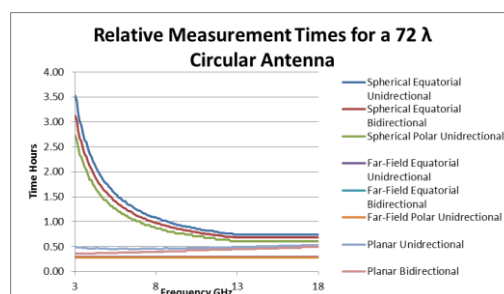


Figure 7 Relative Measurement Times for Different Ranges

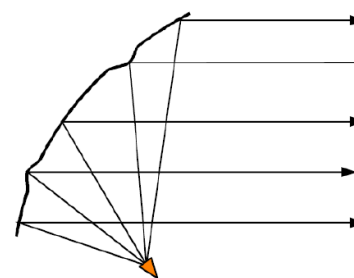


Figure 8 Effect of CATR reflector imperfections

analyse the edges. Method-of-Moment (MoM) techniques have also been successfully developed to analyse CATRs

There are a small number of papers that aim to correct or model the CATR internal coupling effect. The simplest measurement technique is to average the antenna pattern acquired at a number of positions within the quiet zone. There are other models that provide correction of the results.

### 3.2.1.4 Collaboration between partners

This work required collaboration between NPL, LNE and the two universities Rennes 1 and TU Delft. Each party had access and first-hand knowledge of a different type of facility and this work benefitted from their complementary approach.

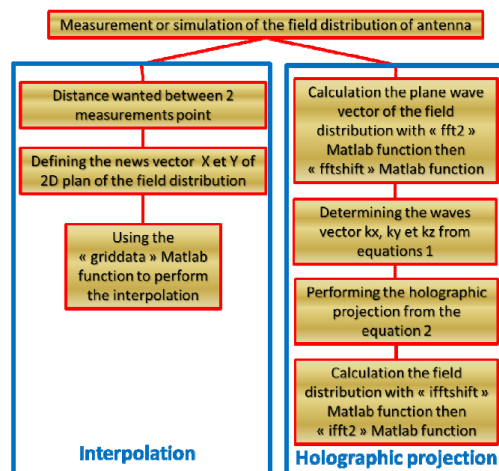


Figure 9 Flow diagram of the interpolation and hologram generation processes

## 3.2.2 Improved antenna test methods using combined measurement and modelling

The aim of this task was to develop methods to speed up EM Field measurements, based on the combination of measurements and predictions. These were then applied to antenna calibration techniques to demonstrate both the techniques identified and to allow these to gain general acceptance.

### 3.2.2.1 Overview of the research importance

Antennas are getting larger with more functions and this is causing unacceptable scheduling delays. Multi-beam antennas in satellites and mobile communications exhibit this trend. The aim was to reduce the number of measurements required while maintaining confidence in the results. Prediction and measurements of antennas beyond the state of the art were required.

This work started with the literature survey outlined in 3.2.1.3.2. Algorithms were designed and tested for the two common geometries: planar and spherical-polar and the results were critically reviewed. It was found that reduced measurement techniques operate in some conditions but not all. For example, compressed sensing removes low-level data which is required for sidelobe predictions.

### 3.2.2.2 Summary of findings

Algorithms were created, tested and the results were critically reviewed for both planar and spherical geometries.

#### 3.2.2.2.1 Planar geometry – simulation and interpolation schemes

The algorithms for the interpolation and holographic projection approaches are illustrated in Figure 9 and Figure 10. A 50 GHz horn, modelled using *CST microwave studio*, was used to test the performance of these strategies. More details of these results are available [17].

The holographic projection method was tested at distances between the antenna and the receiver of 86 mm ( $8\lambda$ ) to 108 mm ( $11\lambda$ ). This method failed for distances of less than 85 mm.

A comparison of the CST and holographic projections showed differences between the results and these errors increase with the separation of the antenna and the receiver. Even

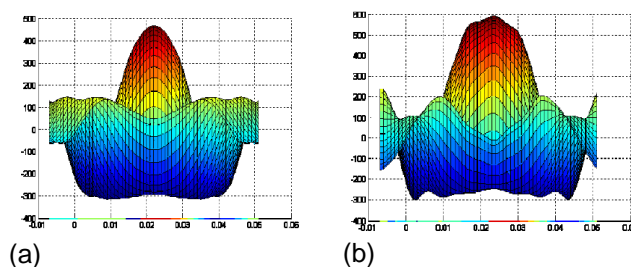


Figure 10 (a) Real part of the field distribution at  $11\lambda$  (CST model) and (b) holographic projection of (a) at  $8\lambda$  showing poor agreement.

the projection of a wave front from  $8\lambda$  to  $11\lambda$  introduces unrepresentative features into the result (see Figure 10).

The interpolation scheme was tested using a linear interpolation scheme as this was the best candidate. Decreasing the point density from a matrix step size of 0.5 mm to 5.0 mm would reduce the size of the dataset by a factor of 100, but the actual interpolation scheme used is critical (see Figure 11).

### 3.2.2.2.2 Planar Geometry measurement test

A 60 GHz antenna measurement performed at the University of Rennes was used to determine the performance of the holographic projection and interpolation methods. The measurement formed a 601x 601 matrix with a grid-spacing of 10 mm over a range of 0 to 600 mm.

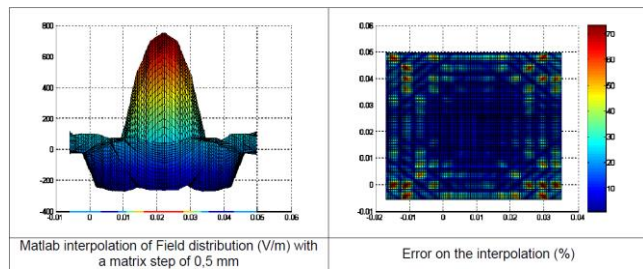


Figure 11 CST Interpolation from 0.5 mm to 5 mm

Both the holographic projection and the interpolation schemes were tested using this data. The measurement data is devoid of sharp discontinuities and the imaginary component is much smaller than the real component. The interpolation approach did not generate the shape differences that were apparent in the earlier test. An explanation for this could be that there are fewer regions exhibiting high curvature and so the linear interpolation is a good fit. This approach can be used to reduce the measurement time without affecting the quality of the results.

The holographic projection method does not appear to provide a good representation of the measured result.

### 3.2.2.2.3 Under sampling antenna measurement for a spherical coordinate system

This work proceeded in two phases. The first phase examined the feasibility of using mode reduction by working with the difference between a measured data set and a predicted data set. The second used an under sampling algorithm based on a limited number of currents flowing on an antenna. This method would not work for the SGH but would work with a simple reflector antenna or an array antenna.

#### 3.2.2.2.3.1 First approach

A horn antenna [18] was used for the measurements and it was modelled using CST Microwave Studio (CST). The agreement between the measured and predicted results was very good and this was improved by realigning the measured pattern. It was found that the SGH could be very accurately represented using a 12-mode data set equivalent to a 15 degree acquisition in theta and phi (see Figure 12). Full details and results are available as a report [19].

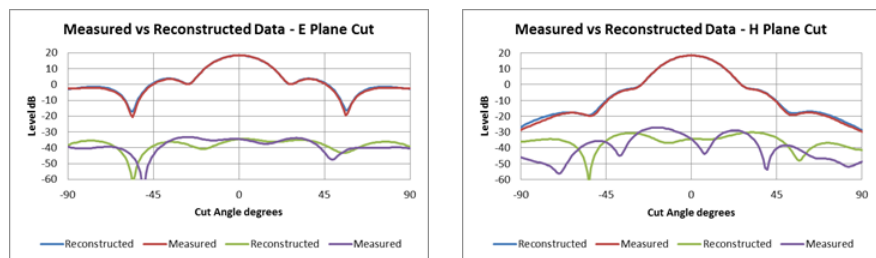


Figure 12 Measured vs reconstructed data

#### 3.2.2.2.3.1 Second approach

The proposed algorithm uses prior knowledge of the currents on the antenna to generate basis functions that could be used to reduce the number of data points needed to predict the antenna radiation pattern. A circular aperture with a  $\phi$ -independent parabolic taper [20] on a pedestal was used, see Figure 13, and this can be represented by:

$$E_x(r') = C + (1 - C) \left[ 1 - \left( \frac{r'}{a} \right)^2 \right]^n \quad (1)$$

where  $N = 3$  and  $C = 10^{-\frac{1}{2}}$ . A Gaussian error was added to the data with an RMS value of -50 dB. The higher the value of  $N$ , the wider the antenna pattern and the lower the value of the sidelobe level. The allowed basis functions were limited to the four unknowns but it was found that the choices were critical for achieving an accurate result. Choosing all the points within the main beam did not predict the sidelobes well.

Figure 14 shows the pattern measured from 4 optimum points. The errors added in have a significant effect on the accuracy of the 'measurement', and Figure 14 shows the worst case error result. The multipath errors are the peak errors across the pattern. Therefore it might be expected that the standard deviation would be  $-50 + 20 \cdot \log(3)$  dB = -40.5 dB. The error is in fact 3 dB above this crude calculation, showing that the method is robust. Figure 14 shows that the antenna pattern calculated from the 4 points has become "depointed".

The example used here was greatly simplified as the excitation was assumed to be an even function, only dependent on the radial dimension of a circular aperture. The excitation of the aperture were defined by 4 components as

$$E = A_1 + A_2 R^2 + A_3 R^4 + A_4 R^6. \quad (2)$$

A conventional spherical acquisition would require 280 points to measure the antenna. The present technique requires 25 points.

This is over an order of magnitude saving in test times. The fitting process predicted the antenna pattern to a peak error below -40 dB in the sidelobe region of the antenna.

The results are critically dependent on the correct choice of basis-functions to describe the pattern. This can be helped by using computational techniques to convert an antenna pattern into the currents on the conducting parts of the antenna. It can also be used for array antennas where the individual array patterns are known. Clearly, errors in the antenna manufacture will affect the resulting pattern and this may not be captured by this approach.

This technique must be specifically applied and only works for antennas where the antenna pattern can be described by a limited number of functions. Despite this, the approach promises many advantages, especially for efficiently performing production testing. Full details of the approach and the results are available as a report [21].

#### 3.2.2.2.4 Summary of the undersampling approaches

For the planar geometry, two undersampling approaches were evaluated, a holographic projection and interpolation. Both of these techniques are data independent. The holographic projection approach appears to be unreliable and introduces errors into the result.

In the planar geometry, the interpolation scheme shows promise but poorly represents areas of field curvature. As a blind method it can reduce the number of measurement points but may also introduce errors due to field curvature. This method could be improved by making a second measurement pass, and sub-sampling areas of high field curvature based on a 2<sup>nd</sup> spatial derivative. Alternatively, the measurement points could be placed using prior knowledge (model-based grid selection).

The two disadvantages of this more complex approach could be the impact of positioning uncertainties and the choice of unevenly spaced data points.

For the spherical polar geometry two undersampling approaches were evaluated. The first described a difference approach where the number of modes could be reduced from 12 modes to 6 modes without significant loss of fidelity. The overall gain of this technique could be up to a factor of four.

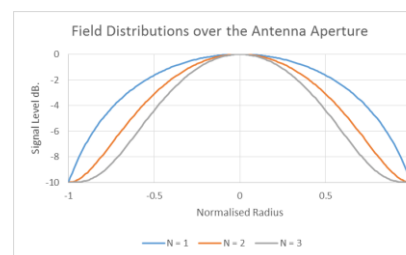


Figure 13 Antenna aperture excitation

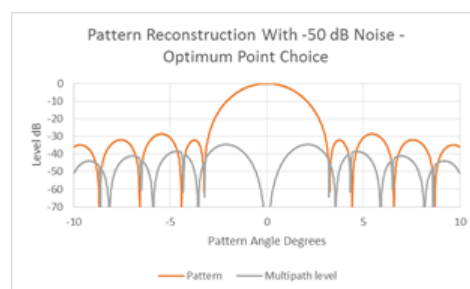


Figure 14 Worst-case error Pattern calculated from optimum choice of points

The second approach used conductive currents on the antenna to calculate the mode pattern. This technique must be specifically applied and only works for antennas where the antenna pattern can be described by a limited number of current or pattern functions. The overall gain is an order of magnitude.

In summary, undersampling techniques applied to planar and spherical-polar can give up to an order of magnitude improvement in the test time. The disadvantage is that the point-placement is not automatic nor have selection rules been defined. Although some of the techniques can be used “blind”, in all cases, a robust and accurate model will provide the information to aid point-placement.

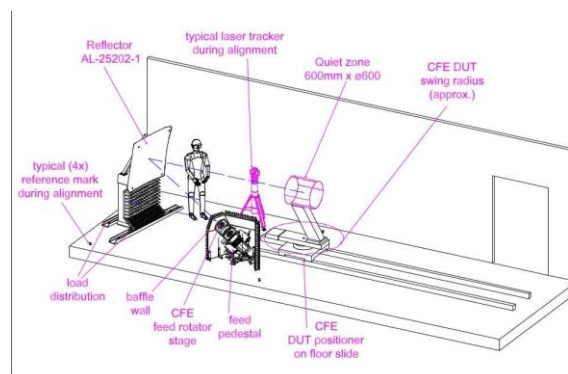


Figure 15 Overall view of the CATR facility

### 3.2.2.3 Collaboration between partners

There has been good collaboration between the consortium members. LNE and U. Rennes 1 worked together on the planar geometry and the results were critically reviewed by TU Delft. NPL worked with U. Rennes 1 on the spherical-polar undersampling.

#### 3.2.3 Improved antenna test method using compact antenna test range (CATR)

The objective of this work was to develop a state of the art Compact Antenna Test Range (CATR) in IETR millimetre wave antenna test facility. In order to achieve this, several tasks must be completed, these were:

1. Design of the system and reflector, shown in Figure 15.
2. Ensuring that the systematic positioning errors in the planar scanner are corrected to yield a software-aligned high-accuracy planar scanner system.
3. The characterisation of the electric field profile within the “Quiet-Zone” (QZ) using an electro-optic probe that does not disturb the field profile.
4. Verification of the scanner performance against other European facilities to demonstrate equivalence.

#### 3.2.3.1 Overview of the research importance

This research is important for three reasons: firstly it provides a high-grade qualified antenna facility that can be used for research and potentially also supports the business community. Secondly, the knowledge, correction algorithms and alignment procedures will be available to set up future CATR systems. Finally, the low perturbation the electro-optic field-probe can be used to test other facilities and the design can be reproduced in other laboratories.

#### 3.2.3.2 CATR facility beyond the state of the art

The new facility has a capability to measure high-gain antennas over the whole millimetre wave range, 30 GHz to 300 GHz, and with a cylindrical Quiet Zone (QZ) volume of 600 mm diameter and 600 mm depth with an axis of revolution aligned on the optical axis of the chamber. The boresight gain of the measured antenna does not suffer much from the quiet zone imperfection but the other parameters such as beam-width and side-lobe level are valuable for antenna design and are strongly affected by the quiet zone shape and stability. Normally the quiet zone nonlinearity is evaluated by simulation and by limited field sampling, which leads to a breach in the traceability of antenna measurement when techniques that combine measurements across the QZ are used. For this system the magnitude taper along the QZ axis will be less than 1 dB and the magnitude of the ripple within the QZ should be less than 0.4 dB. The sum of positioning errors and errors on the mirror surface should give an overall phase ripple of less than 10 degrees, corresponding to a total path error of 28  $\mu\text{m}$  at 300 GHz. The maximum cross-polar requirement (-30 dB) corresponds to a maximum alignment angular rotational of 63 mrad peak-to-peak as the antenna moves across the QZ. The overall performance, limited by the hardware design to 110 GHz, has been extended by software enhancements to 300 GHz. This CATR is based on an existing facility that was upgraded to these higher specifications that exceed the state of the art and the spatial variation of the QZ was calibrated.

### 3.2.3.3 Summary of findings

#### 3.2.3.3.1 Facility and alignment

The chamber section is 3.5x3.05m<sup>2</sup> and the useful distance from the reflector to its feed location must be less than 4m. The chamber optical axis, which is used for the AUT positioning system, is defined by fixed rails in the existing facility as 1.575 m from the ground. The QZ is aligned to this optical axis so that a single coordinate system can be used throughout the design [22].

A laser tracker has been used to provide coarse alignment of the scanning plane, verified by checking several points along the axis. As the accuracy of such a tool depends on the distance between the tracker and the optical target, the alignment may be insufficient at the highest frequencies.

The phase-error specification ±10° is the most difficult to achieve and has three major contributing factors:

- Dynamic range error (linearity error) of the measurement system.
- The thermal drift of the system within the CATR environment
- The positioning error of the probe used for the field measurement.

The chamber environment is temperature controlled to mitigate thermal drift issues. The dynamic range is optimised using a 20 dBi Standard Gain Horn as a field probe [23], and using a low bandwidth IF filter (< 10 Hz) to reduce the noise-floor during measurements. The positioning system is covered in the following section.

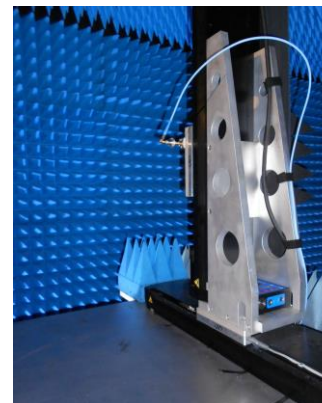


Figure 16 Slide axis and right-hand bracket

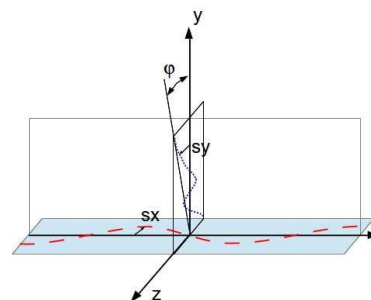


Figure 17 Planarity error

#### 3.2.3.3.2 Positioning system

The variation of phase with frequency was calculated and a value of 5 μm has been chosen as an achievable compromise. The 2D scanner architecture is based on two-high precision slides, Newport Micro-Contrôle model M-IMS 600PP, mounted orthogonally to each other and to the optical axis of the CATR. These have been characterised to work within the design specification. The results were better than the specification e.g. the peak-to-peak on axis accuracy was specified as 20 μm and measured as <3 μm. The chassis was manufactured using 20 mm thick aluminium plate and 80 mm x 80 mm mounts to provide a rigid but light structure (see Figure 16).

The main sources of planarity errors are the pitch angle error and the residual alignment error due to the straightness of each axis. The systematic error associated with the planar scanner was mapped and compensated using the yaw and pitch variation (see Figure 17), using the relation,

$$p(x, y) = y \tan(\varphi(x)) + s_x(x) + s_y(y), \quad (3)$$

where  $x$  and  $y$  are the positions of the respective slide axes, which have associated systematic errors  $s_x(x)$  and  $s_y(y)$ . The  $x$ -slide pitch error is  $\varphi(x)$  and is determined from  $p(x, y)$  by linear regression. An iterative algorithm is used to optimise the estimate for all of the terms. Prior to the correction the residual error was < 200 μm and after this has been measured and the software correction has been applied the absolute planarity error was <(10 ±5) μm, shown in Figure 18.

#### 3.2.3.3.3 Quiet-Zone probing at 60 GHz

QZ probing has been performed using horizontal and vertical field probe orientations and two reflector feed orientations to determine the co- and cross- polarised components. The results

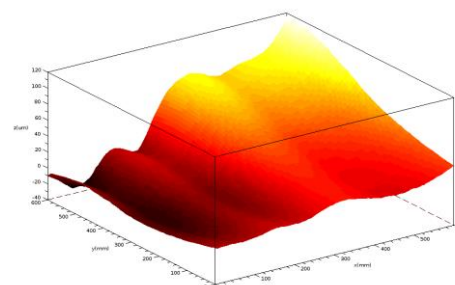


Figure 18 Planarity measurement results: 3D representation

(Figure 19) are very similar for horizontal and vertical polarisations with a variation of  $\pm 0.15$  dB and  $\pm 2.5$  degrees over 80% of the QZ.

**3.2.3.3.4 Further work**

It may be possible to further improve the planarity by including specific shims to improve the levelling. Also, these initial results do not include any errors associated with the RF cable and the rotary joint that has been included to reduce mechanical stresses on the RF connector.

**3.2.3.4 Collaboration between partners**

University of Rennes 1 collaborated with LNE to review the correction algorithm and with PTB to verify the performance of the probe antenna.

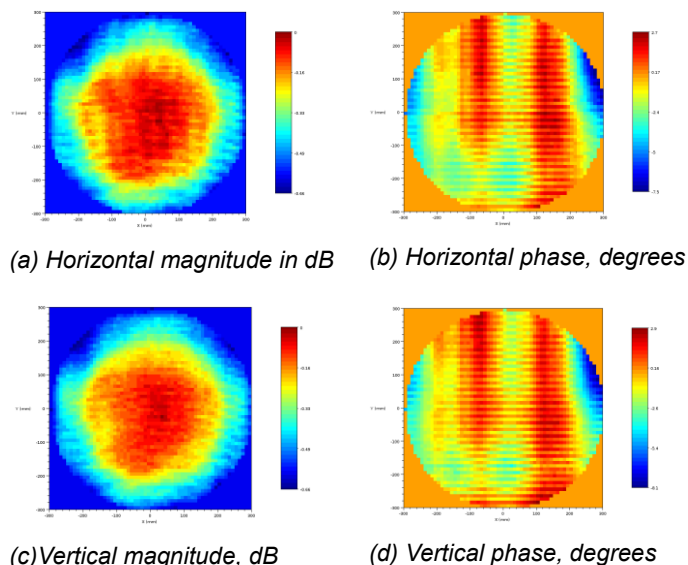


Figure 19 Co-polar Quiet-Zone field probe results

**3.2.4 Low-reflectivity field sampling using an optoelectronic probe**

The objective was to develop an electro-optic probe that provides a minimal disturbance of the RF field close to an antenna system.

**3.2.4.1 Overview of the research importance**

The increased use of mm-wave frequencies for commercial applications provides a drive to reduce test and measurement costs. This can partially be achieved through the increased use of simulation but at some point physical measurement is necessary. At these frequencies the physical size of probe antennas becomes an issue as they significantly perturb the RF fields. The objective to develop an RF sensor that introduces the minimum field perturbation is important as it can be used to characterise simpler RF probes.

**3.2.4.2 Low-reflectivity field-sampling beyond the state of the art**

Multiple reflections between an antenna under test and the receiving antenna constitute a large problem for antenna characterisation. Therefore, it is desirable to develop low reflectivity probes which can be employed for the measurement of the amplitude and phase of antenna patterns. So far, work on low-reflectivity probes focused on dielectric fibres. In this project an optoelectronic low-reflectivity probe made of nonlinear dielectric material has been investigated.

**3.2.4.3 Summary of findings**

A new electro-optic (EO) field sensor that provides minimal disturbance to the electric field has been developed at PTB [24]. This device is capable of measuring the spatially resolved amplitude and phase pattern of GHz and THz antennas. To choose a suitable EO crystal, ZnTe, GaP, GaSe were tested using a W-band source (standard gain horn antenna) using laser

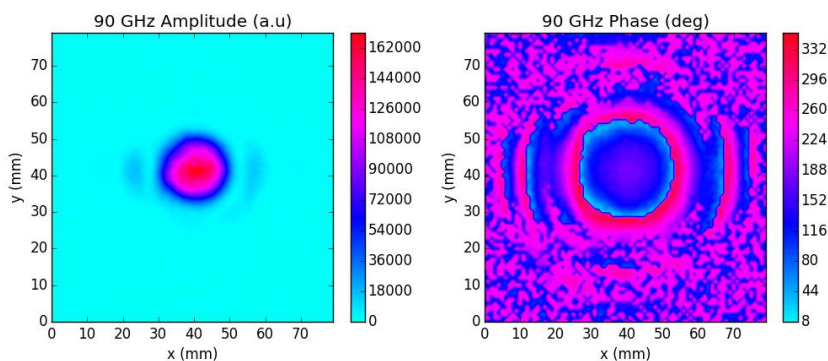


Figure 20 Spatially resolved amplitude and phase of the standard gain horn antenna at 90 GHz obtained from laser-based EO sampling with a distance 60 mm between the antenna and the EO crystal

pulses at 800 nm with a temporal width of 100 fs. We found that zinc telluride (ZnTe) crystals provide the strongest signal and was subsequently used to construct the low-reflectivity EO field sensor.

About 120 test bench measurements have been performed at PTB. In these measurements the AUT was fixed and the EO sensor has been moved performing a planar scan over an area of 80 mm × 80 mm. Figure 20 shows the amplitude and phase measurement results for an antenna. This amplitude data has been obtained after some analysis including background subtraction and squaring of the spatially resolved EO signal, which is proportional to the electric field emitted from the horn antenna.

In addition to amplitude measurements in arbitrary units the EO field sensor has also been calibrated. After calibration quantitative amplitude measurements could be realized. A normalisation constant for our laser based measurements has been obtained from

$$c_1 = \frac{P_{rad}}{\sum_{x,y} I_{x,y}^{meas} \Delta^2}, \tag{4}$$

where  $I_{x,y}^{meas}$  [V<sup>2</sup>] denotes the square of the background-subtracted EO measurement values and  $\Delta$  [mm] is the step size of the two-dimensional scan;  $P_{rad}$  is the total power emitted from the antenna being obtained from measurements using a calibrated radiometer. The sum expresses the summation over all indices of  $I_{x,y}^{meas}$  along the  $x$  and  $y$  directions. The conversion factor  $c_1$  has the unit [ $\mu\text{W} \cdot \text{mm}^{-2} \cdot \text{V}^{-2}$ ] in order to convert  $I_{x,y}^{meas}$  to intensity in SI units [ $\mu\text{W} \cdot \text{mm}^{-2}$ ]. Obviously this normalisation value is just valid for the particular experimental setup and might change considerably once the setup has been realigned.

The normalisation constant can now be used to specify measured intensity distributions in SI units employing the following equation

$$I_{x,y}^{SI} = c_1 I_{x,y}^{meas}. \tag{5}$$

Table 1 Uncertainty budget of the spatially resolved EO amplitude measurements.

Uncertainty source	Relative standard uncertainty	Uncert . Type	Distribution and degrees of freedom
Radiometer measurements $u_{power}$	1.7 %	B	Normal, $\nu = \infty$
Repeatability of EO measurements $u_{repeat}$	3.7 %	A	t-distribution, $\nu = 5$
EO crystal $u_{crystal}$	24 %	B	Rectangular, $\nu = \infty$
Reflections and EO sensitivity of E-field direction $u_{refl}$	15 %	B	Rectangular, $\nu = \infty$
Background $u_{bg}$	3.5 %	B	Normal, $\nu = \infty$
<b>Combined uncertainty <math>u_c, U_c</math></b>	<b>29 % (k=1)</b> <b>58 % (k=2)</b>		

Table 1 shows the overall uncertainty budget for the spatially resolved amplitude measurements. The combined uncertainty is  $u_c = 29\%$  as obtained from the square root of the sum of squares of the individual contributions. In order to calculate the expanded uncertainty with a coverage interval of 95 % ( $k=2$ ) the Welch-Satterthwaite formula has first been used to calculate the effective degree of freedom for  $u_c$ . A value of 1810 has been obtained such that the coverage factor for the expanded uncertainty is exactly 2. This yields an expanded uncertainty for  $c_1$  of  $U_c = 58\%$  [25]

In summary, a low-perturbation EO sampling shows excellent potential for power and intensity measurements at GHz and THz frequencies. Such measurements are important for the development of applications in this frequency range and the technique also helps to enlarge the frequency range of thermal radiometer measurements. Two important goals need to be addressed in more detail. First the invasiveness of the EO crystal in a sampling geometry needs to be further investigated. Moreover the uncertainty components need to be reduced, in particular the uncertainty related to systematic effects. We believe that a reduction of the overall uncertainty by at least a factor of 2 is feasible. It should be pointed out that this technique is not only limited to the measurement of cw radiation but can also be applied to pulsed GHz and THz radiation.

### 3.2.4.4 Collaboration between partners

The design and manufacture of the EO probe was carried out at PTB but the device was used in collaboration with UR1 to measure antenna radiation pattern.

### 3.2.5 Measurement of antennas over a controllable temperature range

A temperature controlled-facility to house test-antennas was developed with a target temperature range of 0 C to 50 C and a volume sufficient to house an antenna of at least 50 x 100 x 200 mm was developed and evaluated in this work.

#### 3.2.5.1 Overview of the research importance

There are many critical communications instances such as satellites, mobile basestations, automotive vehicles and aircraft where the antenna system is cycled over a wide range of temperatures. This is a useful facility to support industry as there are many applications where antennas and active devices will be required to operate over a range of temperatures. This work was carried out by an LNE and Dassault, an industrial partner, showing direct benefit to European industry.

#### 3.2.5.2 Smart antenna measurements beyond the state of the art

A literature survey was conducted [26] prior to the design process and there are several designs [27] that provide a coverage from -50 C to +80 C and for cryogenic temperatures (25 K). In the cryogenic designs, the antenna temperature is controlled through a metallic finger in direct contact with the base of the antenna.

For aeronautics applications most of the tests are performed before and after climate conditioning of the antennas and there is a lack of published information on the antenna performance with the atmosphere variation. The provision of a temperature controlled facility within a European NMI will advance the state of the art. The experimental findings also raise some important points about the performance of these antenna systems in the presence of ice formation.

#### 3.2.5.3 Summary of findings

The preliminary specification was agreed following the literature survey and the thermal enclosure design aimed to achieve the following conditions:

- Sufficient thermal isolation between the surrounding environment (23°C) and the antenna under test.
- The temperature inside the chamber should be homogeneous and controlled by the thermal sensor.
- The thermal chamber should be designed to avoid moisture accumulation on the antenna.
- The material of the thermal enclosure should have a relative permittivity as close as possible to one and be sufficiently strong to a vacuum test.
- Mechanical design should avoid edges and angles that cause diffraction effects.
- The supporting structure must be movable to allow propagation measurement on a horizontal axis.

The chosen test antennas were designed for ATC transponders, operating at frequencies around 1 GHz. The antennas were mounted on a metallic back plane that can be used to facilitate heat flow.

In other work it was found that moisture may lead to condensation and in the worst case to formation of a thin ice-layer on the surface of the antenna. This ice can lead to a dramatic modification of the antenna behaviour and this can be avoided by using a vacuum enclosure or dry air.

The RF transparency of the enclosure is determined by a measurement at ambient temperature. For systems operating at normal air pressure plastic foam, designed for RF applications, is often used as the enclosure material because it has a low impact. Vacuum systems require significant reinforcement and may not be appropriate for large designs. High-density polyethylene can be used at the cost of radome transparency.

The secondary question that this raises is that the ice formation may be representative of the true operating environment.

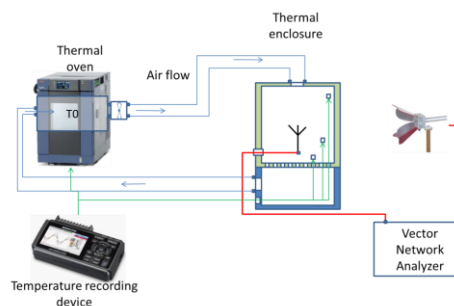


Figure 21 Thermal enclosure system

### 3.2.5.3.1 Design and performance

The objective was to perform measurements of an antenna over a temperature range of 0°C to 50°C in an anechoic chamber, without moisture deposition on the antenna at low temperature and with a minimum perturbation of the RF antenna properties due to the setup. The thermal enclosure consisted of two square/rectangular boxes made of “rohacell” and was connected to the temperature control system by outward and return forced-air ducts that were thermally isolated by a rock wool cover. The heating and cooling was provided by a temperature and humidity chamber that covered the temperature range from -40°C to 150°C. The thermal losses were such that the outflow from the thermal oven system must an output range from -30 C to +75 C to achieve the desired 0 C to 50 C within the radome. The temperature cycling time to achieve 0 C or 50 C was 240 minutes and 80 minutes respectively. The system is shown in Figure 21 and the performance in Figure 22.

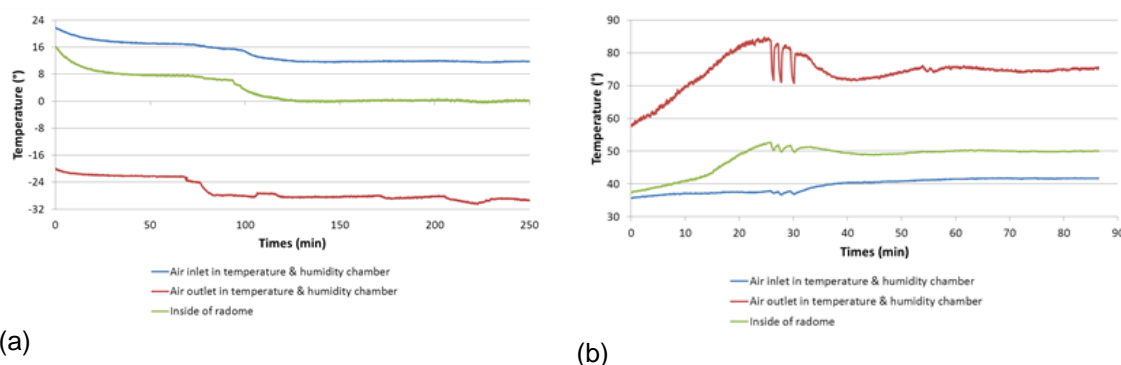


Figure 22 Temperature variation with time to achieve 0 C (a) and 50 C (b)

### 3.2.5.4 Collaboration between partners

This work was performed as a collaboration between LNE and Dassault. The initial benefit is for the European avionics and space industries, particularly SMEs that cannot afford such facilities. A secondary benefit is the dissemination of the results to the project partners.

## 3.3 Optical Communications

The aim was to develop novel and reliable measurement techniques to optimise optical transmitters commonly implemented as double nested Mach-Zehnder modulators to generate the complex modulation formats to meet the continued technology growth in optical communications that support the core network. The two activities that we believed would have the greatest impact were a traceable method, with supporting user guides, to measure the single and balanced photoreceivers that form the core of the coherent systems. The second activity was targeted to provide better or improved the digital metrics.

### 3.3.1 Characterisation of photoreceiver systems

The aim of this task was to characterise complex frequency response of a single photodiode from approximately 1 GHz with a bandwidth of at least 100 GHz and Common-Mode response within an orthogonal system comprising two photodiodes. Matched photodiodes are a key element for the coherent optical communication systems.

#### 3.3.1.1 Overview of the research importance

Research plan to provide a calibration capability to measure single-ended photodiode vector frequency-response 1-100 GHz with traceability to Electro-Optic Sampling (EOS) provides a capability to separate the performance of the transmitter and receiver elements.

The extension to characterise the behaviour of balanced differential photodiodes supports the development of the hybrid coherent receivers that are a key component of > 100 GHz optical communications.

### 3.3.1.2 Characterising photoreceiver systems beyond the state of the art

The development of a fully traceable vector frequency-response capability over 1-100 GHz within an NMI is beyond the state of the art in Europe.

The measurement and analysis of frequency response, group delay and vector difference frequency response of balanced differential photodiodes, together with a simple means of characterisation using EOS or DSO is beyond the state of the art.

### 3.3.1.3 Summary of findings

#### 3.3.1.3.1 Single-Ended photodiodes and receivers

The characterisation of photodiodes (PDs) is challenging since its bandwidth often exceeds the bandwidth of the utilised measuring devices. Previously, PDs have been characterised using a combination of an electrical vector network analyser (VNA) and laser-based electro-optical sampling techniques up to a frequency of 110 GHz [28]. We have employed an all-optical method for the characterisation of PDs using a recently developed laser-based VNA [29]. With this instrumentation, we are able to measure both, the time- and frequency domain responses.

The basic concept of the laser-based VNA is shown in Figure 23. Ultrashort voltage pulses with frequency components exceeding 500 GHz are generated on a coplanar waveguide (CPW) by means of a femtosecond laser (pump beam). The voltage signals are detected via electro-optic sampling employing the electro-optic effect of the GaAs substrate on which the CPW is fabricated. Sampling the voltage pulses at two different positions on the CPW, the reflection coefficient at the measurement plane can be calculated, which in turn also allows for the measurement of scattering parameters [29] with a dynamic range of more than 40 dB and a bandwidth of up to 500 GHz.

The PD under test has a nominal bandwidth of 100 GHz (*XPDV4120R, u<sup>2</sup>t/Finisar*). The voltage pulses created by the PD need to be transferred to our CPW measurement plane. The PD characterisation is then a two-step process. First, we characterise the coaxial-coplanar link as shown in Figure 23a, using our laser-based VNA. In particular we obtain the scattering parameters  $S_{11}$  and  $S_{12}$  as indicated in Figure 23a. A detailed description of this measurement will be deferred to another publication. Second, we determine the voltage pulses created by the PD at the CPW measurement plane  $V_{CPW}$  and the reflection coefficient  $\Gamma$  as indicated in Figure 23b. The PD's voltage at the calibration plane (see Figure 23c for the definition of the calibration plane) is then given by

$$V_{PD} = \frac{V_{CPW}}{S_{12}Z_R H_{EOS}} \frac{(1-S_{11}\Gamma)}{(1+\Gamma)}, \quad (6)$$

with the second term on the right-hand side accounting for multiple reflections (full mismatch within the measured time window) and  $H_{EOS}$  denoting the transfer function of electro-optic sampling. The impedance ratio  $Z_R$  considers that  $V_{PD}$  and  $V_{CPW}$  are voltages and not power waves [30]:

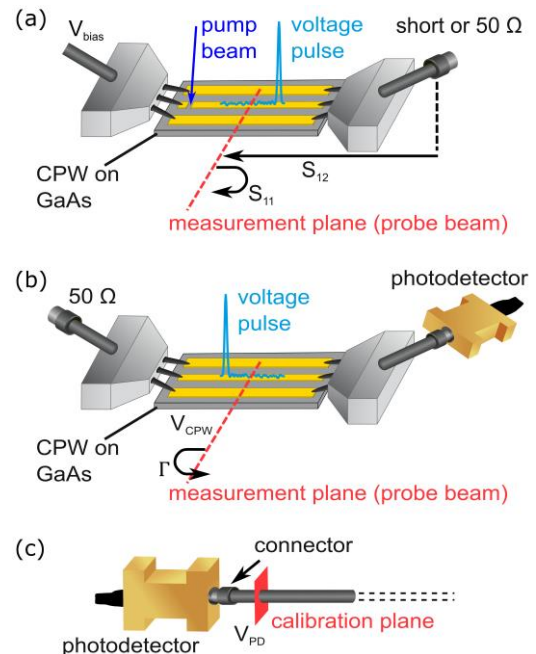


Figure 23 (a) Schematic setup for determination of  $S_{11}$  and  $S_{12}$ . (b) Schematic setup for determination of  $\Gamma$  and  $V_{CPW}$ . (c) Calibration plane of the PD, which is placed right after its coaxial connector.

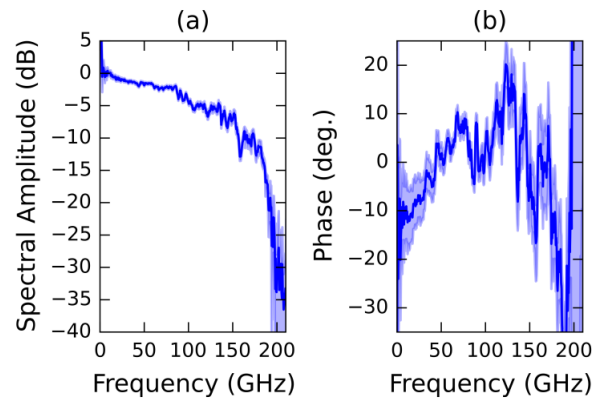


Figure 24 Amplitude (a) and phase (b) spectrum of the single PD at the calibration plane. The amplitude spectrum was normalized to 0 dB at 10 GHz. A linear slope from 10 GHz and 200 GHz was subtracted from the phase to appreciate any nonlinear dependence.

$$Z_R = \left| \frac{Z_{CPW}}{50 \Omega} \right| \sqrt{\frac{50 \Omega}{\text{Re}\{Z_{CPW}\}}}, \quad (7)$$

where  $Z_{CPW}$  is the complex characteristic impedance of the CPW [29]; the impedance of the coaxial line is taken as 50 Ω.

The amplitude and phase of  $V_{PD}$  in the frequency domain are shown in Figure 24. The relative amplitude drops to -10 dB at 170 GHz and frequency components up to about 260 GHz were obtained. This emphasises that also frequencies above the single-mode frequency of the coaxial line (110 GHz) contribute considerably to the spectrum. In order to investigate this influence in more detail we show in Figure 25 the time-domain shape of  $V_{PD}$  calculated from the full spectrum and from a spectrum whose frequency components above 110 GHz were cut off using a Butterworth filter. Clearly the altered spectrum leads to a broader pulse shape as well as additional oscillations.

The increased uncertainty at very low frequencies (<10 GHz) results from the limited frequency resolution, i.e., limited time window, of the laser-based measurements. For further studies an asynchronous sampling technique seems to be a promising candidate to improve the accuracy and uncertainty at low frequencies.

### 3.3.1.3.2 Oscilloscope measurements

Three single-ended photodiodes and a photoreceiver were tested using a Digital Sampling Oscilloscope (DSO). The optical source can be phase-locked to an external synthesiser and so the timebase correction algorithm could be applied to remove jitter and correct for timebase nonlinearity.

The laser repetition frequency varies from day to day e.g. 19 998 063 Hz (MENLO) but the system can be stabilised and locked to a 10 MHz reference signal. The bandwidth of this source covers 1540 nm to 1610 nm giving about 100 fs pulse width. This travels through an optical fibre to get to the device under test, broadening the optical source to about 2.9 ps. Ideally, the optical spectrum should be restricted to about 10 nm to minimise the pulse spreading in the optical fibre (about 800 fs at the photodiode over 3 metres of SMF28 single-mode fibre). The system is shown in Figure 26. The IQ and comb frequencies are harmonically related to the trigger through different (unrelated) integer values. This avoids any distortion of the IQ signal creating phantom terms within the comb lines [31].

For the photodiodes and DSO the microwave impedance match was also measured and applied as a correction. The photodiode response extends beyond the specified frequency range of the APC3.5 connectors. The impedance-match corrected results, shown in Figure 27, give a good result at up to 33 GHz, suggesting that there are some high-order components present (over-moded connector).

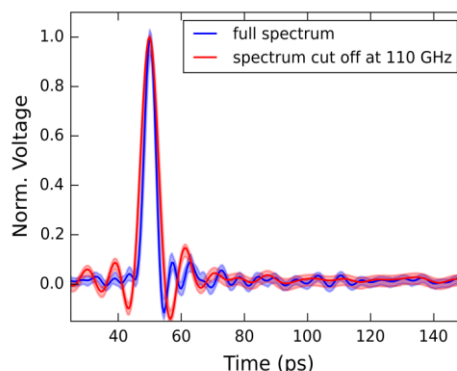


Figure 25. Impulse response of the single PD extracted from the full spectrum and from a reduced spectrum where the frequency components above 110 GHz were cut off using a Butterworth filter. The 95% confidence intervals are marked by the light semi-transparent colours

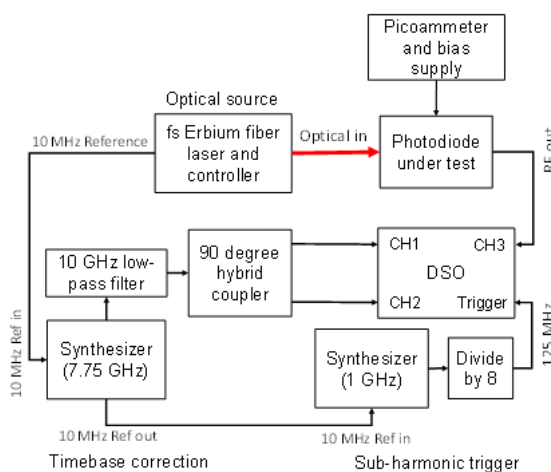


Figure 26 Measurement system layout showing the configuration of the DSO

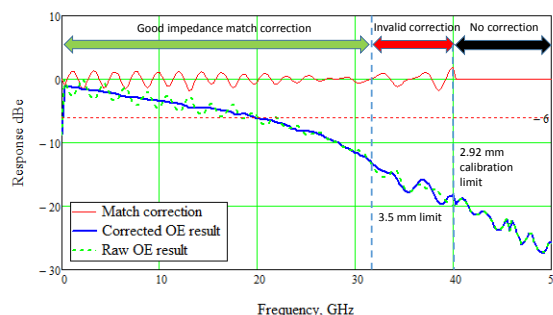


Figure 27 Frequency-domain response of HP83440C photodiode with impedance match correction

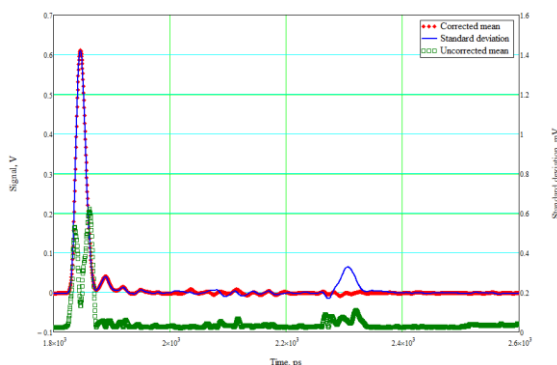


Figure 28 Time-domain match-corrected response of the HP83440D photodiode

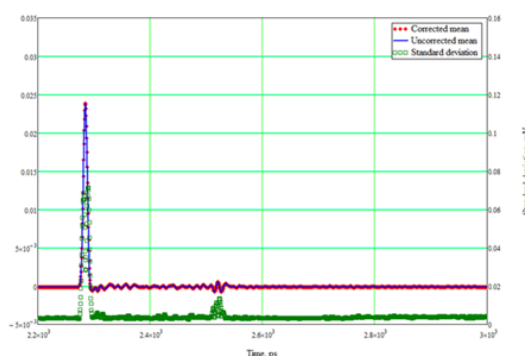


Figure 29 Keysight 86116B O/E Receiver response

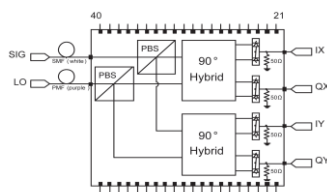
The match correction removes the dominant reflection coefficients and improves the result. The uncertainties have been propagated using the compact covariance software. The uncertainty components in the time-domain are higher in the slope regions of the impulse, suggesting that the residual timebase, drift corrections or jitter is not fully compensated and so the diode bandwidth will be higher than measured but the standard deviation values are small, so this is a minor problem. The time-domain response and uncertainties are shown in Figure 28.

The Agilent 86116B receiver can be treated in the same way as the photodiode except that as the photodiode and sampler are intimately coupled and so there is no impedance-match correction required. This instrument has the full sampler bandwidth available. The response and uncertainties are shown Figure 29.

### 3.3.1.3.3 Differential photodiode common-mode characterisation



(a) Optical hybrid device



(b) Optical hybrid layout

Figure 30 Commercial Optical hybrid and internal configuration

Balanced photodetectors [32], [33] and [34] are key precursor to hybrid detectors used for coherent communications see Figure 30). Such coherent devices with 64 Gbaud data rate are commercially available [35] and proof-of-principle operation of 1.92 Tbaud over 225 km using polarisation-multiplexed optical time-division multiplexing with a 170 GHz optical channel data rate have been demonstrated [36].

We addressed the common-mode rejection-ratio (CMRR) characterisation of a balanced high-speed photodetector [32], [33] and [34]. The test device (*BPDV2150R, u<sup>2</sup>t/Finisar*) has a nominal bandwidth of 43 GHz and is representative of the devices used in current systems. We also determined the CMRR of the test device using a Digital Sampling Oscilloscope (DSO) and a Vector Network Analyser (VNA) with the aim of finding the limitation of such approaches.

The optimised results show that the photodiodes are well matched in terms of the RF performance in order to achieve a high level CMRR across the band, greatly exceeding the specified performance of 15 dB. It is important to note that the maximum CMRR does not always occur when the photocurrents are exactly equal. This may influence the best practice for active optical alignment of coherent detectors if the "best" result can be achieved by minimising the RF power when both devices are illuminated.

The standard definition for CMRR used for electrical components, such as operational amplifiers is

$$CMRR = 20 \log \left( \frac{V_p - V_n}{V_p + V_n} \right), \tag{8}$$

where  $V_p$  and  $V_n$  are the positive and negative voltage inputs, respectively. This definition is satisfactory for electronic systems where the common-mode input is applied to both inputs simultaneously by connecting the

two inputs together, but in a high-bandwidth differential photodiode, the two devices require optical power to separately illuminate the two photodiodes. The detrimental CMMR issue arises from three potential sources:

1. The same optical power applied to the input connector may experience different delays or losses in the optical fibre coupling.
2. If the optical fibre losses are corrected and the photocurrent for the two photodiodes is balanced then there is the potential that cross-coupling or light-absorption in undepleted material will result in slight differences in  $I^{(f)}/I_{(dc)}$ . Light absorbed in undepleted material causes a minority carrier concentration gradient and, as the material is highly conductive, there is little field gradient. These carriers will contribute to the dc or low-frequency response but not the high-bandwidth response of the device. Balancing the photocurrents gives an imbalance in the device responses so that the CMRR is not at its maximum value.
3. The limiting value for CMRR is when the frequency response difference between two devices is minimised. The responses of the two photodiodes may differ, particularly if part of the optical signal is absorbed in undepleted material. As a consequence, matching the dc photocurrents may not provide the best rejection of high-bandwidth common-mode signals. The main contributing factor to CMRR over a wide bandwidth is the difference between the frequency-response of the two photodiodes. This can be optimised by minimising the normalised error.

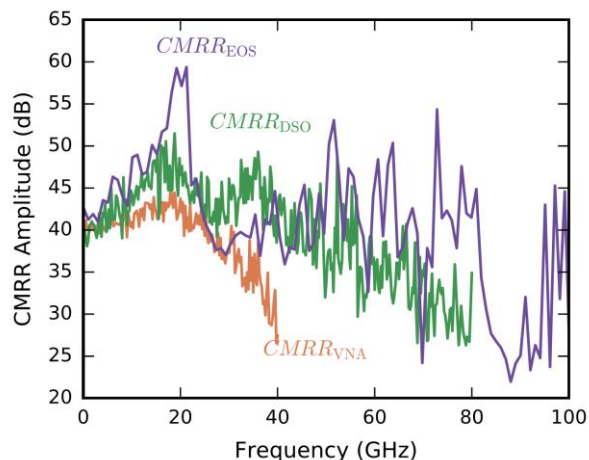


Figure 31 Comparison of the CMRR obtained with the three different techniques. The coverage intervals have been omitted for clarity

To account for these imperfections we allow for small changes of the positive voltage by an amplitude factor and a phase factor  $\tau$  such that the optimised positive voltage is given by

$$V'_p(f, \alpha, \tau) = \alpha \exp(j\omega\tau) V_p(f), \tag{9}$$

with  $\alpha$  and  $\tau$  being chosen to minimise

$$E_{min} = \min_{\alpha, \tau} \sum_f \left| \frac{V'_p(f, \alpha, \tau) + V_n(f)}{V'_p(f, \alpha, \tau) - V_n(f)} \right|, \tag{10}$$

where the summation over  $f$  is done in a frequency range where  $V_p(f)$  and  $V_n(f)$  provide significant power. The error term is the reciprocal of the core element of the CMRR calculation. This has been chosen because the sum term will greatly exceed the residual noise and uncertainty components whereas the difference term may be comparable, for a high CMRR device. This also allows the use of simple expansions to treat the correlated terms.

The CMRR obtained with the three different techniques is shown in Figure 31. Measurements with commercial DSO and VNA systems show that these instruments can measure a CMRR of at least 40 dB but the upper frequency limit is significantly less than that available with the EOS. The VNA covered the lowest bandwidth due to the 20 GHz optical modulator and the low RF power used (-7 dBm), whereas the DSO was useable beyond its specified upper-frequency because the measurement is ratiometric and the RF connectors were not disturbed during the measurement.

The curves of Figure 31 show reasonable agreement. The differences between the DSO and EOS results above 70 GHz most likely results from the limited bandwidth of the DSO. Similarly the lower VNA result above 30 GHz is due to the low bandwidth of the optical modulator. It should be noted that the optimised CMRR depends on the optimisation bandwidth and, thus, also on the frequency spectrum of the measured voltage pulses. We

believe that this dependence is the origin of the differences between the DSO and EOS results at approximately 20 GHz.

The critical dependence of the CMRR value on linear instrument corrections, such as waveform time-alignment and timebase correction suggest that these additional corrections are necessary to achieve a high CMRR result. The photodiode measurements were restricted to about 150 mV peak. The diode can be used at higher pulse levels, with the risk of some nonlinearity from the device under test or from the DSO.

In summary, a CMRR system comprising of commercial instrumentation, such as a DSO and optical pulse source or a VNA, DFB and high-bandwidth modulator can be realised. The results compare well to measurements using EOS techniques based on femtosecond lasers, which will even allow the methods using commercial instrumentation to be optimised.

#### **3.3.1.4 Collaboration between partners**

There was successful collaboration between NPL, PTB and Finisar, formerly u<sup>2</sup>t, (collaborator) during the device measurements. Finisar provided loan devices following the failure of the NPL component during the comparison.

There was also an unofficial collaboration between NPL and the University of Sussex to access their mode-locked laser system and deliver the work after the failure of the laser system at NPL.

#### **3.3.2 Characterisation of high-speed transmitters for advanced optical modulation formats using coherent detection**

The aim of this task was to implement an optical IQ transmitter with wide-bandwidth RF amplifiers and to characterise the modulator using an optical constellation analyser. This task also established the relationship between EVM and other related parameters such as quadrature imbalance and timing-skew including an uncertainty analysis.

In addition, characterising the behaviour of the DRTO and the O/E device was part of the drive to determine the linearity and waveforms within the system.

#### **3.3.2.1 Overview of the research importance**

The optical IQ transmitter, wide-bandwidth RF amplifiers and optical modulators together form the heart of the communications system.

During the research phase electrical Arbitrary Waveform Generator and the Digital Real-Time Oscilloscope (DRTO) form the equivalent electrical-electrical link. It is therefore essential to also be able to separate the electrical source and receiver, especially for higher-order QAM signals where linearity is important. The DRTO is a key instrument in this system and so developing a sound calibration framework for this instrument was an important element for this work.

Developing an understanding of the relationship between Bit Error-Ratio and EVM is important for future system maintenance and operation as it provides equivalence between two key instrumentation approaches.

#### **3.3.2.2 Characterisation of high-speed digital and coherent measurements beyond the state of the art**

At the time that this work was started there was no manufacturer independent calibration capability for DRTO, which is at the heart of the coherent transmission system. The prime-number algorithm was the state of the art to calibrate these instruments.

The DRTO samples at 100 GSa/s and so if the data rate is 25 GSa/s then each symbol will be represented by only four samples. Within the algorithm used by Chalmers the data is resampled at two points per symbol. The careful choice of repetition and sampling rates for the AWG and DRTO allows the evolution of the optical waveform to be captured in greater resolution, so that nonlinear elements can be found and eliminated. This has been demonstrated and is beyond the current state of the art.

The algorithm developed to relate EVM with BER is a valuable way to compare diagnostic tools for high-speed optical communications. This work is beyond the state of the art.

### 3.3.2.3 Summary of findings

#### 3.3.2.3.1 Bit Pattern Generation and traceability for DRTO

The Primary EOS system is normally used to calibrate high-speed DSO and these instruments are then used to cross-calibrate pulse-generators and other DSO's. There is no reason why the traceable DSO or the EOS system cannot be used to directly calibrate a DRTO.

The high-speed DRTO uses multiple ADC, which will be closely, but not perfectly matched. This leads to a series of sub-Nyquist tones where the lowest subharmonic ( $f_{sp}$ ) will be at a frequency

$$f_{sp} = \frac{S}{m'} \tag{11}$$

Where  $S$  is the sample-rate and  $m$  is the number of ADCs.

It is most beneficial to use an externally locked reference and a known stimulation from a pulse generator to determine the impulse response. The measurable epoch is not only defined by data-record length considerations but also by phase-stability, see Figure 32. The minimum averaging time and frequency should also be chosen so that there is an integer relationship between the number of cycles ( $R$ ) of  $f_{CW}$  and the number of time samples ( $P$ ) in the averaging period. The selection is based on prime-number pairs that have no common prime-factors. The acquired waveform contains  $n$  points and comprises  $Q$  repeats of  $P$  periods and that the comb frequency passes close to one of more of the sub-Nyquist tones. As the results are transformed into the frequency domain the choice of  $P$  should avoid large prime numbers. For example a near 100 MHz comb can be achieved on a DRTO operating at 80 GSa/s and choosing  $P$  as 25599 ( $3 \times 7 \times 23 \times 53$ ) and  $R$  as 32. The result is 3.906 kHz away from the 100 MHz target. For a captured epoch of  $10^6$  samples there will be 39 repeats and 1639 unused samples

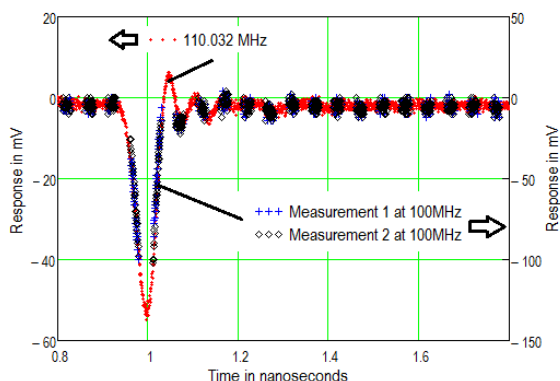


Figure 34 Pulse response for degenerate and nondegenerate signals measured using DRTO C as separate measurements. The residual timing variation (100 MHz) is insufficient to fully represent the waveform.

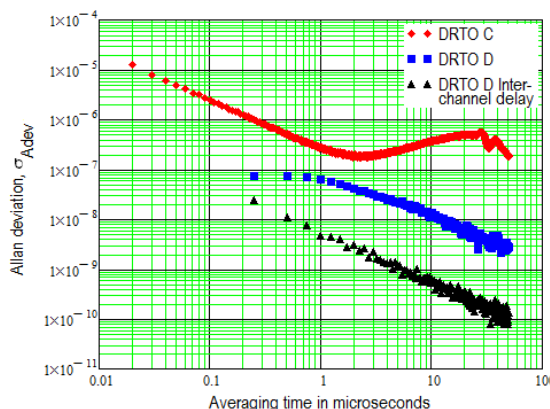


Figure 32 Phase locking must be achieved over the full epoch to avoid truncation errors. For DRTO C this must be less than 2.6  $\mu$ s

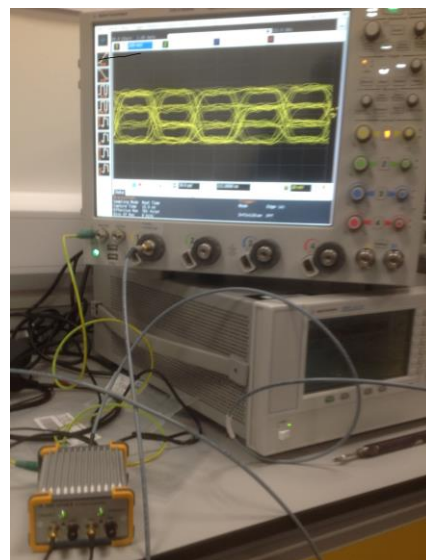


Figure 33 High-quality eye diagrams from SHF Driver (NPL)

A single acquisition is sufficient to calculate the frequency response and uncertainties.

Another way of viewing this result is that for the simple case, e.g. 100 MHz exactly, the full waveform contains 800 points and this may be insufficient to represent a 30 ps electrical pulse (2.4 points). If instead the full epoch requires 32 cycles then using modulo arithmetic the same pulse is now represented by 77 points. See Figure 34 for a similar example.

### 3.3.2.3.2 Implement optical IQ transmitter

The aim was to implement an optical IQ transmitter with wide-bandwidth RF amplifiers and to characterise the modulator using an optical constellation analyser. The initial tests were performed using an SHF amplifier, which provided equal slew-rates for rising and falling edges and a higher voltage output.

The modulator systems at NPL were evaluated using a Keysight N4392A Integrated Optical Modulation Analyser. This allowed real-time analysis of the constellation diagrams and to develop a familiarity with the instrument.

Initial measurements were made at NPL using a 25 GHz SHF826H modulator and the 12 GSa/s AWG to investigate waveform pre-distortion using the optical receiver as the detector (see Figure 33 and Figure 38).

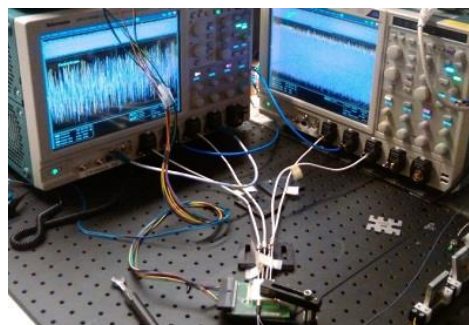


Figure 35 Optical receiver at Chalmers University Photonics Laboratory

### 3.3.2.3.3 Optical waveform metrology (real-time sampling) to characterise IQ transmitter

The majority of the measurements were made at Chalmers University using the GHz two RTDO at 100 GSa/s (see Figure 35) and an Arbitrary Waveform Generator at 56 GSa/s (Keysight M9502A, Variable rate). For certain PRBS sequences this allowed the acquired data to be folded to give a detailed representation of the waveform (see Figure 36). At 28 GBaud (DAC rate is 56 GBaud, with 2 points per cycle), the RTDO is cyclic (25 points correspond to 7 symbols). This is important for multi-level signals where the system linearity affects the errors in the constellation diagram, and hence the EVM.

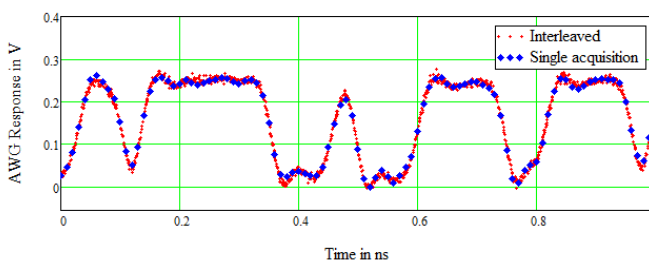


Figure 36 Single acquisition (blue) and interleaved acquisition (red) using the prime-number relationship between the AWG and RTDO sampling rates

### 3.3.2.3.4 EVM Measurements and uncertainty analysis

The measurement arrangement at Chalmers University is shown in Figure 37. The optical signal was a PRBS11, PRBS 15 or PRBS17 pseudorandom bit pattern with QPSK, DP-QPSK or DP-16QAM modulation and Gaussian ( $\beta = 0.1$ ), Rectangular or Raised Root-Cosine (RRC) filters with ( $\alpha = 0.1$  or 0.5) on both the transmitter and the receiver (DP stands for Dual Polarisation). The data rate was varied from 10 GBd to 32 GBd. A pre-distortion correction was applied to the signal based on known properties of the transmission path (Chalmers University in-house code). Various impairments were introduced to the system (gain imbalance, quadrature error, IQ skew) and the constellation was observed at the transmitter output using the Keysight N4392A (position ②, dashed line). The signal at the transmitter output was regarded as “ideal”. Then the N4392A (Figure 39) was re-connected in order to measure the same signal as the coherent receiver comprised of the intradyne coherent receiver ( $u^t$  64 GBd photodetector) and two Tektronix DPO 73304D oscilloscopes (Figure 35) with 100 GS/s sampling rate (position ③). To test the amplifiers’ distortion, several signal acquisitions were also made in position ①). To determine the system performance and for further analysis of EVM-OSNR-BER dependency with various impairments,

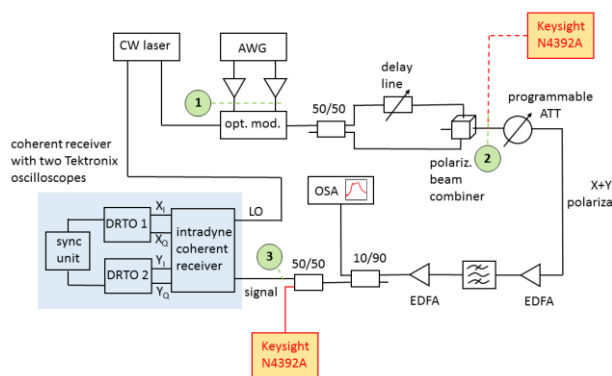


Figure 37 Measurement setup for the EVM and BER measurement. Short optical fibre was used between the transmitter and receiver, thus nonlinear fibre effects and polarization dispersion have only small effect on the signal quality.

an OSNR sweep has been performed for each settings. All instruments were free-running without a 10 MHz external reference. Any frequency difference between the clocks was negligible even on the longest epoch (50 microseconds).

EVM has been widely used as one of parameters defining the performance of wireless communication equipment. It is defined as the magnitude of the difference between the reference waveform and the measured waveform in a vector diagram as follows:

$$EVM_{rms} = \sqrt{\frac{\sum_{n=1}^N |S_n - S_{0,n}|^2}{\sum_{n=1}^N |S_{0,n}|^2}} \quad (12)$$

where  $S_n$  is the normalised  $n^{th}$  symbol in the stream of measured symbols,  $S_{0,n}$  is the ideal normalised constellation point of the  $n^{th}$  symbol and  $N$  is the number of unique symbols in the constellation. These differences are averaged over a given, typically large number of symbols  $T \gg N$  and are often shown as a percent of the average power per symbols of the constellation.

Assuming that the system errors are mainly due to optical AWGN (neglecting nonlinear effects and electrical noise) and the receiver is data-aided then

$$EVM \approx \frac{1}{\sqrt{SNR}} = \sqrt{\frac{N_0}{E_s}}, \quad (13)$$

where the SNR is the signal-to-noise ratio and  $N_0/E_s$  is the inverted signal to noise ratio for an M-ary modulation system. In this work, optical signal-to-noise ratio (OSNR) measured in a 12.5 GHz bandwidth was used and related to the SNR. For a M-ary modulation with coherent detection in a Gaussian-noise channel with perfect recovery of the carrier frequency and phase and raised-cosine pulse-shaping at the data rate the BER is given by,

$$BER = \frac{2(L-1)}{L \log_2(L)} \operatorname{erfc} \left( \sqrt{\frac{3 \log_2(L)}{L^2-1} \frac{2 E_s}{N_0 \log_2(M)}} \right), \quad (14)$$

where  $L$  is the number of levels in each dimension of the M-ary modulation system. For the Gaussian noise model  $N_0$  and hence EVM can be re-written in terms of the in-phase  $n_{I,t}$  and quadrature  $n_{Q,t}$  noise components and the power of the normalized ideal or transmitted constellation giving

$$BER = \frac{2(L-1)}{L \log_2(L)} \operatorname{erfc} \left( \sqrt{\frac{3 \log_2(L)}{L^2-1} \frac{2}{EVM_{rms}^2 \log_2(M)}} \right). \quad (15)$$

Signal impairments, such as gain imbalance  $g_t$  and quadrature error  $\varphi_t$  are directly connected and including the relationship between SNR and optical SNR (OSNR) we get

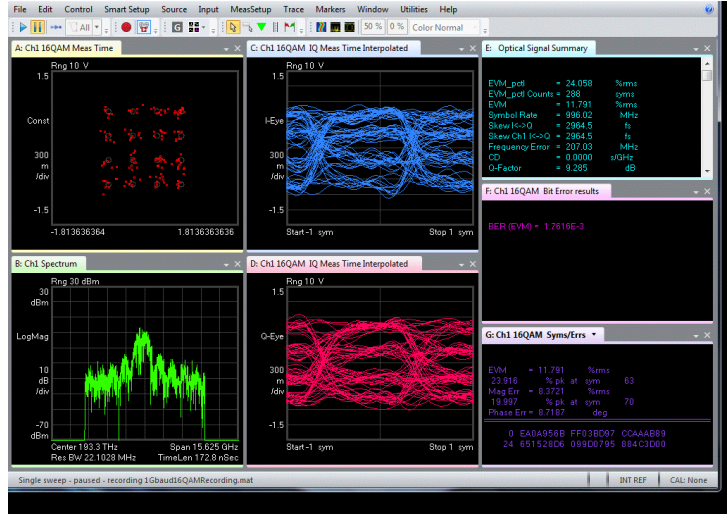


Figure 38 Real-time EVM analysis using Keysight N4392A of 16 QAM IQ measurement at 1 Gsa/s



Figure 39 Measurement of a DP-QPSK signal using the Keysight N4392A unit

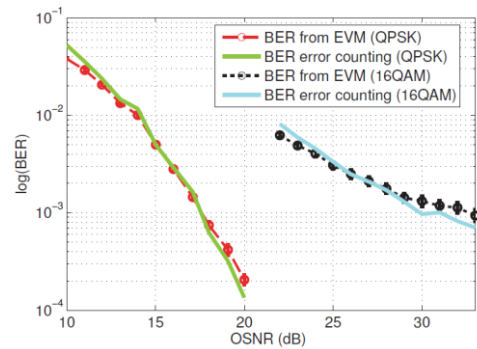


Figure 40 Agreement between the BER determined by error counting and calculated from EVM. QPSK (timing skew = 12 ps) and 16QAM (gain imbalance = 1.5 dB) modulation, 28 GBd, X-polarization.

$$EVM_{rms} = \sqrt{\frac{RM}{B OSNR} + 2 - (1 + g_t) \sqrt{\frac{1 + \cos(\varphi_t)}{1 + g_t^2}}}, \quad (16)$$

Where B is the OSNR measurement bandwidth, R is the bitrate and M is the number of constellation points.

The optical EVM was measured using two different instruments (Keysight N4392A and two Tektronix DPO 73304D oscilloscopes). In both cases, the optical signal is first converted to an electrical base band signal using a coherent receiver. The N4392A allows to measure the EVM in real time with 4095 symbols in one batch. The oscilloscope measurement procedure is slower, but more controllable giving reliable EVM results as a higher number of symbols, typically 250 k, were analysed. The maximum measurable EVM, using a blind receiver, is 44.5% for QPSK and 12.1% for 16QAM.

The BER was calculated by direct error-counting and compared with the values estimated from the EVM. As there is significant internal signal processing involved in the acquisition and re-sampling of the data, the EVM measurement is not always unique, as it depends on the settings of DSP algorithm, which are not always available for users of commercial measurement equipment. Thus the BER calculated from EVM might slightly differ from the reality. Despite that, the BER conversion from EVM is robust for broad range of applied impairments (gain imbalance, timing skew, and quadrature error). The results are shown in Figure 40 and Figure 41. The EVM measurement is significantly faster than the currently used offline processing for a reliable computation the bit error ratio (BER), especially if the signal quality is high.

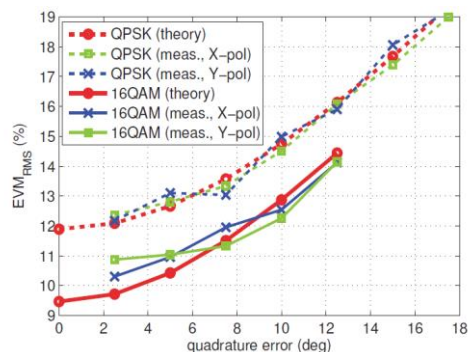


Figure 41 Agreement between the theoretical EVM and measured values calculated determined by error counting and calculated from EVM

### 3.3.2.4 Collaboration between partners

The main participants in this work were PTB, NPL, CMI, Keysight and Chalmers University. The photonic testbed located at Chalmers University was used by NPL and CMI to develop and verify the relationship between BER and EVM. Staff at Chalmers provided training on the operation of the testbed system and facilitated its use. This was a successful collaboration and additional information was provided to Chalmers to allow a better estimation of the system component performance.

### 3.4 Key scientific results

In particular, the scientific results achieved within this project are:

- Traceable RF field measurements for LTE supporting a new calibration service
- Available MIMO systems within NMIs and a better understanding of the digital measurement issues
- Two algorithms to reduce the test-time for smart antenna systems
- Validated near-field to far-field transforms
- A non-invasive electro-optic sensor for RF field measurement
- Demonstration of equivalence between CATR, spherical polar and planar near-field antenna facilities
- A state-of-the-art CATR facility in Europe
- Thermal test environment for avionic antenna testing
- A detailed study of undersampling techniques for antennas showing which methods do not work
- A photodiode and photoreceiver calibration capability for > 100 GHz components
- Methodology and calibration capability for >50 GHz dual photodiodes for coherent communications
- Calibration algorithms for real-time digital oscilloscopes to avoid instrument impairments
- Invention of new modulation scheme for communications [37]

#### 4 Actual and potential impact

In terms of the overall need for the project, the European Commission identified the need to invest in high-speed connectivity and services to compete internationally and generate wealth for its citizens. Specifically the partners and industry supporters of the project identified that access to traceable metrology is vital for development of communication technologies. The steering, dissemination and exploitation activities were chosen to provide the highest impact where possible.

##### 4.1 Direct impact activities undertaken

###### 4.1.1 Advisory Board

An advisory board for the Consortium was drawn from the key project stakeholders. Their objective was to ensure that the research remained well focussed on the industrial needs. To achieve this they participated in our review meetings and suggested improvements to increase the impact of this project. As a consequence of their recommendations we joined the following standards groups:

1. CTIA (USA) Over-the-Air measurements (MOTA) and uncertainty sub-group (MUSG). These groups are actively developing standards for over-the-air (OTA) measurements and are relevant to the terrestrial and MIMO measurement effort. The majority of their work programme had already been set and so our participation did not involve active measurement but rather provided insight into the measurement issues from an industrial perspective.
2. The ETSI Industry Specification Group on millimetre-wave transmission (ISG mWT) is key for taking forward the high-bandwidth transmission for point-to-point links for high-bandwidth back-haul and the future mm-wave needs of 5G. We attended two plenary meetings and have participated in the development of work-items.

There were five board members drawn from key industries and standards groups.

- ESA (European Space Agency)
- ETSI (European Telecommunications Standards Institute)
- Keysight Technologies
- Finisar (formerly U<sup>2</sup>t Photonics AG)
- Real Wireless (formerly NEC / Mobile VCE / ICT KTN)

###### 4.1.2 Newsletters

Four newsletters were prepared and electronically distributed in May 2014, April 2015, November 2015 and June 2016, outlining recent results and future events (see Table 2). The newsletters are available on the website and were circulated to the Advisory Board, stakeholders and collaborators. The final newsletter was longer and provided a summary of the highlights achieved in each technical area of the project.

Table 2 Newsletter technical articles

May 2014
LTE Power Measurements
Characterisation of antennas
Characterisation of ultrafast photodiodes
April 2015

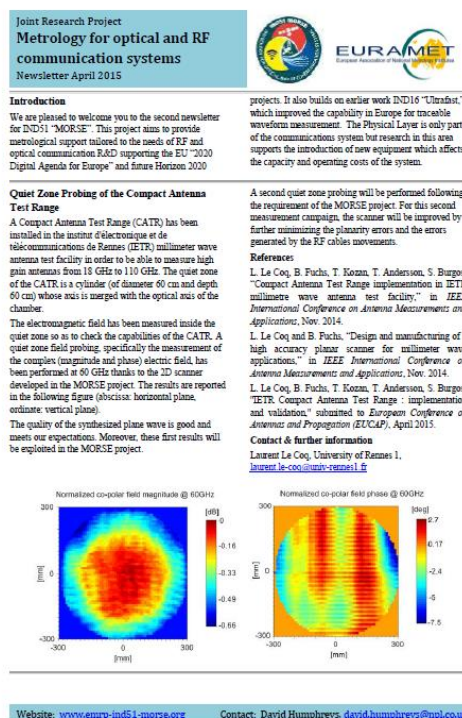


Figure 42 Sample newsletter page (April 2015)

Quiet Zone Probing of the Compact Antenna Test-Range

High-speed optical communication measurements at Chalmers

Characterisation of MIMO antenna

November 2015

Metrology for High-Speed Optical QPSK and 16-QAM Coherent Transmission at Chalmers University, Sweden

Near Field Setup for Millimetre-Wave System Embedded Antennas

Antenna reference for signal processing assessment

#### 4.1.3 Conference presentations

Conference presentations reach the relevant community more directly and to allow direct feedback, we chose the most suitable presentation at international conferences (academic community) and national conferences (engineering design communities, authorities) and through the EU COST programme. During the project we joined COST IC 1004 attending two meetings and giving a presentation. We were also involved in COST IC1102 attending and presenting at one meeting. The COST meetings are attended mainly by academics and students with some industry participation. Much of the information shared is pre-publication. The impact benefit is through knowledge transfer to the students.

At the outset we identified the conferences with high potential impact but we were not able to access all of these because of the timing of the results. Overall we delivered seventeen international conference papers which exceeded the target to deliver at least nine presentations. The digest copies are electronically searchable using IEEE Xplore.

#### 4.1.4 Journal publications

Conference and Journal papers provide one of the most accessible media to disseminate the technical outputs from the project. These outputs were aimed at the international academic and engineering design communities. The target was to submit at least four international journal papers for publication. One of the key criteria was that the journals should be searchable electronically using IEEE Xplore or Web of Science in addition to the Euramet repository requirement. Overall the project team were prolific producing a total of seven accepted journal papers.

#### 4.1.5 Best practice guides and other protocols and procedures

To facilitate best practice amongst the end-user communities and other European NMIs we have prepared seven best-practice guides which are available in an electronic version on the project website.

**Table 3 Summary of Best Practice guides**

Title	Author	Date
Guidelines for the evaluation of uncertainties when measuring LTE signals with diode-based sensors	Soumya Sunder Dash	Nov. 2015
Sensitivity of LTE $R_0$ measurement with respect to multipath propagation	Frederic Pythoud	Nov. 2015
Efficient measurement of smart antennas	Tian Hong Loh, David Cheadle	June 2016
Guidelines for the alignment of a scanner inside a compact range for the measurement of Quiet-Zone field	Laurent Le Coq, Benjamin Fuchs	June 2016
Improving the Acquisition Time in Spherical Near-Field Measurements	Philip Miller	June 2016
Guidelines for the full-waveform characterisation of photodiodes using sampling oscilloscopes	David Humphreys	June 2016

4.1.6 Trade journals and popular press

Trade journals have high circulation figures and are accessible throughout industry. Two trade journal articles have been published in trade journals, IEEE Spectrum [38] and METinfo [39].

4.1.7 Input to standardisation

The Consortium had already established links to several standardisation activities. Not all of the originally planned activities proved to be valuable. During the course of the project the Advisory board made recommendations and facilitated joining new and highly relevant groups.

Table 4 Contribution to standard activities

Standards Committee / Technical Committee / WG	Relevance/success
International Electrotechnical Commission (IEC)	TC85 WG22: Good contributions TC86 WG4: Less relevant
Deutsche Kommission Elektrotechnik, DKE, Komitee 964 Cost IC 1004 - Group SWG1.1: Antennas - Group: TWGO-OTA (over the air testing) CTIA (USA) facilitated by the advisory board	Good contribution, attended meetings. Presentation at two meetings. Good contributions.  Joined over the air testing (MOTA) and measurement uncertainties subgroup (MUSG) during the project. Attended by telephone meetings. Valuable contribution providing insights into measurement issues.
ETSI Industry Standards Group on millimetre-wave transmission (mWT) facilitated by the advisory board	Joined mWT during the course of the project. Attended plenary meetings and telephone meetings. Good contributions.
IEEE P1765 - Recommended Practice for Estimating the Uncertainty In Measurements of Modulated Signals for Wireless Communications with Application to Error Vector Magnitude and Other System-Level Distortion Metrics	Joined this group close to the end of this project. Good contributions
International Telecommunications Union (ITU)	ITU-T SG15 Monitor/observer  ITU-T SG15 Q6 A project partner contribution to Q6 throughout the period of the project

4.1.8 Workshops

4.1.8.1 **“Do’s and Don’ts for mm-wave antenna characterisation” - Keysight Insight Seminar Series**

TU Delft and Keysight Technologies, together with other universities and companies in the Netherlands within the Netherlands Antenna Research Framework (NARF), organised a workshop on antenna measurements. This full-day seminar comprised ten presentations of which at least five demonstrated the research outputs from this project. In addition there was a demonstration of mm-wave VNA measurements and a tour of the TU Delft facilities.



Figure 43 IETR presentation at TU Delft - Keysight seminar 21<sup>st</sup> April 2015

#### 4.1.8.2 Final one-day workshop 9<sup>th</sup> June 2016

A one-day dissemination workshop was held at NPL on Thursday 9<sup>th</sup> June 2016 (Figure 44). There were fourteen oral presentations and eight posters where the research results from the project were presented and discussed. The attendance (33) was lower than anticipated but the material from the majority of the presentation is available on the web-page either as static or web presentations.



Figure 44 Final one-day meeting at NPL, UK

#### 4.1.9 Training and dissemination

The training and dissemination activities were selected to best suit the local needs within the countries of each project partner. As a consequence the activities and dissemination strategies were quite varied ranging from high level with small numbers of postgraduate students or NMI staff to broader presentations to national science and engineering societies.

#### 4.1.9.1 Dissemination

At a national level, local language conferences and technical meetings were often informal allowing greater discussion and the incorporation of training elements and the group focus could range from engineering to business, such as local knowledge networks. The aim was for each project partner to provide at least one presentation or training element per year to benefit the European scientific and engineering community within their country. This was exceeded as the total number of training and local presentations was over forty. Examples of the variety are shown in Table 5. In addition, within the university partners, the postgraduate students working on this project received additional training over a period of months.

#### 4.1.9.2 Web courses and other dissemination routes

Three web courses, each focussing on a different technical aspect of the project, are available from the final one-day meeting. These are available for download from the project website.

Table 5 Examples of dissemination to industry, academics and the public within this project

Description	Audience size	Date
Project overview to ICT KTN, Wireless Technology & Spectrum working group meeting, UK	10-25 industry and academic	6 Mar. 2014
Presentation to 41 <sup>st</sup> meeting of the Czech Elektrotechnical Society, subgroup Microwave technique, Czech Republic	80 mainly industry	19 Nov. 2014
46 <sup>th</sup> session of the PEGESS group (Prüfstellen-Erfahrungsgemeinschaft für EMV, Sachschutz und elektrische Sicherheit), Switzerland	26-50 mainly industry	18 Mar. 2015
Training and scientific exchange with project team staff from UK and Czech Republic at Chalmers University, Sweden	4 professional metrologists	March 2015
Seminar presentation, "Der Femtosekundenlaser als Samplingoszilloskop und Netzwerkanalysator", Germany	>100 industry and academic	March 2015
Poster presentations at Congrès International de Métrologie, Paris, France	26-50, scientific and research	22-24 Sept. 2015
Presentation to 43 <sup>rd</sup> meeting of the Czech Elektrotechnical Society, subgroup Microwave technique, Prague, Czech Republic	80 mainly industry	18 Nov. 2015

In addition to the web material, several other electronic methods were tested. A Linked-In group was formed for the project but this approach received very few hits and was not viewed as successful. Cambridge Wireless

offer the ability to post event notices on their website. As a Founder Member, NPL made use of this to promote the project activities to a large group within the UK.

Several of the project participants are members of ResearchGate [40], a professional social-networking website for research science. Papers submitted to the Euramet repository were also uploaded by project participants with a ResearchGate profile. The site allows the output of other scientists to be monitored and new papers are flagged by this process, leading to increased awareness. The ResearchGate activity, although not in the original plan, was viewed as successful.

#### 4.1.10 Exploitation

##### 4.1.10.1 Intellectual property

This project has generated knowledge that has been publicly disseminated and private IP associated with the measurement facilities, algorithms and services. This will benefit European science and engineering, and hence European citizens.

##### 4.1.10.2 Commercialisation

As a result of this research the NMI partners have used the results in a variety of ways to support the external European customers. New capability has been added to existing facilities, new facilities have been developed and new capability has enabled further research projects. The potential for commercialisation of the facilities and potential services will be assessed by the individual partners. In some cases, for example, it is possible that a commercial calibration service will not be viable but the support for European science and engineering will come from direct collaboration with industry or by enabling further research using the equipment developed here.

Table 6 Summary of current commercialisation

Description	Exploitation	Location
LTE power measurement service for electric field probes	Commercial calibration service	Switzerland
Software-defined radio system 2 x 2 MIMO, for operation to 6 GHz	Core system to underpin 5G mm-wave research. Validated for direct and Over-The-Air measurements. Economic use as a service to be assessed.	UK
Upgraded CATR system with known Quiet-Zone profile and motion compensation algorithm and methodology with propagation of uncertainties	Research system available for University Rennes 1 and commercial use	France
Upgraded planar scanning system with undersampling algorithm	Research system available for Technical University Delft and commercial use	Netherlands
Electro-optic sampling system for electric field probing to > 100 GHz	Research use. Potential for calibration and measurement to be assessed	Germany
Thermal enclosure for antenna measurements	Developed for work with the avionics industry. Potential as a measurement service to be determined	France
Traceable calibration methodology for Digital Real-Time Oscilloscopes	Algorithms published and the commercial viability of a measurement service to be assessed	UK
Traceable measurement of photodiodes 1-100 GHz using EOS with uncertainty analysis	System available and the commercial viability of a measurement service to be assessed	Germany
Traceable measurement of Dual photodiodes 1-70 GHz using EOS with uncertainty analysis	System available and the commercial viability of a measurement service to be assessed	Germany
Traceable measurement of Dual photodiodes 1-50 GHz using Digital Sampling Oscilloscopes	System available and the commercial viability of a measurement service to be assessed	UK
EVM/BER relationships	Algorithms will inform future standardisation of digital metrics through IEEE P1765 standards committee.	UK/ USA/ Czech Republic

#### **4.2 Actual and Potential impact**

Future telecommunications growth depends on the development and delivery of new technology. This project developed traceable measurement infrastructure and modelling techniques for mobile, satellite and optical communications to minimise the time it takes to test and improve new devices, and therefore reduce time to market. Traceable measurement for signal and power output from devices ensures conformity to standards and safeguards end users. New measurement techniques for rapid characterisation of optical components allows industry to monitor device performance. The project outputs allow the project partners to make a useful and valid contribution to the current 5G Research activity.

#### **4.3 Early uptake**

This project developed facilities within European measurement institutes and universities that are now available for use by industry to train future engineers and to provide NMI with a better insight into practical measurement issues in the field.

The Software defined radio system has been used to underpin the Euramet EMRP MET5G research.

During the term of the project the RF power LTE measurement scheme was tested with industry and a report provided to the Swiss government to inform regulation. In addition, four commercial RF power calibrations have already been carried out by METAS using their new calibration system based on the validated software.

Quintel joined the consortium as a collaborator and provided antennas for test. This greatly helped the assessment of undersampling strategies. Their take-up of the technology has been put on hold because of loss of key staff.

Software correction algorithm enhanced compact-range antenna facility at the University Rennes 1, in France has been enhanced using technology developed in this project.

Early uptake of the 2x2 MIMO Software-Defined Radio facilities developed at NPL are already creating impact for 5G research in the UK through the Euramet EMRP MET5G project.

#### **4.4 Wider and long-term impacts**

The relationship between Error Vector Magnitude, EVM has been established and will be included in submissions to the IEEE P1765 Group.

One of the partners played an active role with ITU in the group SG15 Networks, Technologies and Infrastructures for Transport, Access and Home, to answer "Q6" which relates to several optical transport standards, such as Contribution on EVM calculation methods according to amendment G.698.2. This has an ongoing and worldwide impact.

A project partner has contributed to IEC TC85 WG22 through the preparation of a technical annex for standard IEC62754 "Computation of Waveform Parameter Uncertainties". This has an ongoing and worldwide impact.

A project partner has contributed to the ETSI mWT pre-standard in areas of use-cases for mm-wave in a future telecommunication system.

There has been good collaboration between Finisar (formerly U<sup>2</sup>T), PTB and NPL on the measurement of the high-bandwidth photodiodes used for optical communications, which has the potential to be used in new products.

A serendipitous impact that occurred during the development of the LTE RF power service was the invention of a new modulation scheme to increase the transmission bitrate with a given SNR. This unexpected result has been presented in a conference [37].

## **5 Website address and contact details**

[www.emrp-ind51-morse.org](http://www.emrp-ind51-morse.org)

Dr David Humphreys

National Physical Laboratory

+44 208 943 6389

[david.humphreys@npl.co.uk](mailto:david.humphreys@npl.co.uk)

## References

- [1] "A growth package for integrated European infrastructures," COM(2011) 676, [http://ec.europa.eu/commission\\_2010-2014/president/news/speeches-statements/pdf/20111019\\_1\\_en.pdf](http://ec.europa.eu/commission_2010-2014/president/news/speeches-statements/pdf/20111019_1_en.pdf)
- [2] T. Gill "Flexible Spectrum – Implications for Radio Technology", ICTKTN Sept. 2011, [https://connect.innovateuk.org/web/spectrum/document-library?p\\_p\\_id=20&p\\_p\\_lifecycle=0&p\\_p\\_state=maximized&p\\_p\\_mode=view&ns\\_20\\_struts\\_action=%2Fdocument\\_library%2Fview&ns\\_20\\_folderId=5047402](https://connect.innovateuk.org/web/spectrum/document-library?p_p_id=20&p_p_lifecycle=0&p_p_state=maximized&p_p_mode=view&ns_20_struts_action=%2Fdocument_library%2Fview&ns_20_folderId=5047402)
- [3] P. Fritschi et al., "Workshop LTE; Funktechnik, Messtechnik, Regulation; Forschungsstiftung Mobilkommunikation, ETH Zürich;."
- [4] H. Liu, S. Gao, T. H. Loh and F. Qin, "Low-cost intelligent antenna with low profile and broad bandwidth," in IET Microwaves, Antennas & Propagation, vol. 7, no. 5, pp. 356-364, April 11 2013. doi: 10.1049/iet-map.2011.0398
- [5] T. H. Loh and D. Cheedle, "Measuring adaptive beamforming smart antennas," IND51 MORSE Final One-day Workshop, Teddington, UK, 9<sup>th</sup> June 2016.
- [6] T. H. Loh, P. Miller and B. Fuchs, "Antenna Pattern Measurement: - Antenna Software Modelling Packages," EMRP IND51 "MORSE" Deliverable Report: D2.1.1, Jan 2014.
- [7] P. Miller, B. Fuchs, "Antenna Pattern Measurement: - Under Sampling Strategies," EMRP IND15 "MORSE" Deliverable Report: D2.1.2, Nov. 2013.
- [8] T. Hastie, R. Tibshirani and J. Friedman, "The elements of Statistical Learning," Stanford University, Springer Books, Feb. 2009.
- [9] N. A. C. Cressie, "Statistics for Spatial Data," (Revised Edition), New York, John Wiley and Sons, 1993.
- [10] R. Gerchberg, "Super-resolution through error energy reduction," Optical Acta, Vol 21, no 9, pp 709–720. 1974
- [11] A. Papoulis, "A new algorithm in spectral analysis and band-limited extrapolation," IEEE Trans. Circuits Syst., CAS-22, pp. 735–742, Sept 1975.
- [12] C. Cappellin, A. Frandsen, S. Pivnenko, G. Lemanczyk and O. Breinbjerg, "Diagnostics of the SMOS radiometer antenna system at the DTU-ESA spherical near-field antenna test facility," The Second European Conference on Antennas and Propagation (EuCAP), pp. 1- 6, 2007.
- [13] Wasim Q. Malik, Hammad A. Khan, David J. Edwards, and Christopher J. Stevens, "A Gridding Algorithm for Efficient Density Compensation of Arbitrarily Sampled Fourier-Domain Data," IEEE Sarnoff Symposium on Advances in Wired and Wireless Communication, Apr. 18-19, pp. 218
- [14] A. Dutt and V. Rokhlin, "Fast Fourier transforms for non-equispaced data," SIAM J. Scientific Comput., vol. 14, pp. 1369–1393, Nov. 1993
- [15] Technische Universität Chemnitz website: <http://www-user.tu-chemnitz.de/~potts/nfft/>
- [16] Benjamin Fuchs, Laurent Le Coq and Jean-Marie Lerat, "Literature search to investigate CATR test models and coupling formulation between quiet zone field and source," EMRP IND51 "MORSE" deliverable report D2.1.5, July 2014.
- [17] M. Charles, "Report of the MORSE project for holographic distribution and data interpolation," EMRP IND51 "MORSE" Deliverable report D2.2.5, Apr. 2015.
- [18] Flann Microwave WG17 SGH Model No 17240-20.
- [19] P. Miller, "Antenna Pattern Measurement: - Initial Algorithm Trial," EMRP IND51 "MORSE" Deliverable report D2.2.7, Jan. 2015.
- [20] W. L. Stutzman and G. A. Thiele 1981. *Antenna Theory and Design*. pp 420-421. New York. Wiley
- [21] P. Miller, "Antenna Pattern Measurement: - Improved Algorithm Trial," EMRP IND51 "MORSE" Deliverable report D2.28, Mar. 2016.
- [22] L. Le Coq, B. Fuchs, "High-accuracy planar scanner facility designed and manufactured with software, alignment method and quantification procedures," Deliverable report EMRP IND51 D2.3.2, July 2014
- [23] L. Le Coq and B. Fuchs, "Probe antenna and radiation pattern data," EMRP IND51 "MORSE" Deliverable report D2.3.1, July 2014.
- [24] H. Fuser and M. Bieler, "Terahertz Frequency Combs," J Infrared Milli Terahz Waves 35, 585–609 (2014).
- [25] Y. Deng, H. Fuser, and M. Bieler, "Absolute Intensity Measurements of CW GHz and THz Radiation Using Electro-Optic Sampling," IEEE Transactions on Instrumentation and Measurement 64, 1734–1740 (2015).
- [26] J.-M. Lerat, "Thermal enclosure literature review and Design specification," EMRP MORSE Deliverable Report, D2.5.1, Mar. 2014.

- 
- [27] L.J. Foged, A. Giacomini, R. Morbidini, "Thermal testing of antennas in spherical nearfield multi-probe system", Eucap, 2011.
- [28] D. F. Williams et al., "Covariance-Based Uncertainty Analysis of the NIST Electrooptic Sampling System," IEEE Trans. Microw. Theory Tech., vol. 54, no. 1, pp. 481–491, Jan. 2006.
- [29] M. Bieler, H. Fuser, and K. Pierz, "Time-Domain Optoelectronic Vector Network Analysis on Coplanar Waveguides," IEEE Transactions on Microwave Theory and Techniques, vol. 63, no. 11, pp. 3775–3784, Nov. 2015.
- [30] R. B. Marks and D. F. Williams, "A General Waveguide Circuit Theory," J. Res. Natl. Inst. Stand. Technol., vol. 97, no. 5, pp. 533–562, Oct. 1992.
- [31] D. Humphreys, "Best Practice Guide for dual-photodiode Common-Mode Rejection-Ratio measurements using commercial Digital Sampling Oscilloscopes," Best-Practice Guide.
- [32] Y. Painchaud, M. Poulin, M. Morin, and M. Têtu, "Performance of balanced detection in a coherent receiver," Opt. Express, vol. 17, no. 5, pp. 3659–3672, Mar 2009.
- [33] X. Jin, J. Su, Y. Zheng, C. Chen, W. Wang, and K. Peng, "Balanced homodyne detection with high common mode rejection ratio based on parameter compensation of two arbitrary photodiodes," Opt. Express, vol. 23, p. 23859, Sep. 2015.
- [34] A. Beling, H. G. Bach, D. Schmidt, G. G. Mekonnen, M. Rohde, L. Molle, H. Ehlers, and A. Umbach, "High-speed balanced photodetector module with 20db broadband common-mode rejection ratio," in Optical Fiber Communication Conference. Optical Society of America, 2003, p. WF4.
- [35] Webpage of Finisar Corporation. [Online]. Available: [www.finisar.com](http://www.finisar.com)
- [36] D. O. Otuya, K. Kasai, T. Hirooka, and M. Nakazawa, "Coherent Nyquist orthogonal TDM transmission with a spectral efficiency of 10.6 Bit/s/Hz," Journal of Lightwave Technology, vol. 34, no. 2, pp. 768–775, Jan 2016.
- [37] S. S. Dash, F. Pythoud, B. Baeuerle, A. Josten, P. Leuchtmann, D. Hillerkuss, J. Leuthold, "Receiver Algorithm for Decoding Constellation Modulation," in proc. Advanced Photonics Congress, Vancouver, 18-21 Jul. 2016
- [38] D. McCormick, "Femtosecond Lasers Drive a New Generation of Network Vector Analyzers," IEEE Spectrum, 16<sup>th</sup> Nov. 2015. Available at <http://spectrum.ieee.org/tech-talk/at-work/test-and-measurement/femtosecond-lasers-drive-a-new-generation-of-network-vector-analyzers>
- [39] Soumya Dash and Frederic Pythoud, "A reference setup to calibrate LTE Code selective field probes," METinfo, vol. 23 no. 1, 2016. Available at: <https://www.metas.ch/dam/data/metas/Dokumentation/METASPublikationen/metinfo/METinfo2016/A%20reference%20setup%20to%20calibrate.pdf>
- [40] ResearchGate. Available at <http://www.researchgate.net/>

## 6 List of publications

The following list of references of work published by the project team are available directly from the publisher and through the Euramet repository.

1. D. A. Humphreys, M. Hudlicka, I. Fatadin, "Calibration of wideband digital real-time oscilloscopes," Conference on Precision Electromagnetic Measurements 2014 (CPEM 2014), pp.698 - 699, 24-29 Aug. 2014.
2. Y. Deng, H. Fuser, M. Bieler, "Absolute intensity measurement of a 100 GHz source using laser-based electro-optic sampling," Conference on Precision Electromagnetic Measurements 2014 (CPEM 2014), pp.748 - 749, 24-29 Aug. 2014
3. M. Hudlicka, I. Fatadin, D. Humphreys: Analysis of high-speed optical data transmission using advanced modulation formats (original title in Czech: Analýza vysokorychlostních datových přenosů s vícestavovými optickými modulačními formáty), 41<sup>st</sup> meeting of the Czech electrotechnical society, subgroup Microwave technique, 19<sup>th</sup> Nov. 2014, Prague, Czech Republic, pp. 1-4, ISBN 978-80-02-02541-2
4. I. Fatadin, D. Ives, S. J. Savory, "Carrier-Phase Estimation for 16-QAM Optical Coherent Systems Using QPSK Partitioning With Barycenter Approximation," IEEE J. Lightwave Tech., vol. 32, No 13 pp. 2420 - 2427.
5. T. H. Loh and W. Qi, "A comparison of MIMO antenna efficiency measurements performed in Anechoic Chamber and Reverberation Chamber", Digest of 85<sup>th</sup> Microwave Measurement Conference (ARFTG), Phoenix, USA.
6. L. Le Coq, B. Fuchs, T. Kozan, T. Andersson and Sara Burgos, "Compact antenna test range implementation in IETR millimetre wave antenna test facility," IEEE Conference on Antenna Measurements & Applications (CAMA), 2014, Antibes Juan-les-Pins, 2014, pp. 1-4.
7. L. Le Coq and B. Fuchs, "Design and manufacturing of a high accuracy planar scanner for millimeter wave applications," IEEE Conference on Antenna Measurements & Applications (CAMA), Antibes Juan-les-Pins, 2014, pp. 1-4.
8. Y. Deng, H. Fuser, M. Bieler, "Absolute Intensity Measurements of CW GHz and THz Radiation Using Electro-Optic Sampling," IEEE Trans. on Instrumen. and Meas., vol. 64, no. 6, pp. 1734 - 1740, Jun. 2015.
9. D. A. Humphreys, Martin Hudlička and Irshaad Fatadin, "Calibration of Wideband Digital Real-time Oscilloscopes," IEEE Trans.on Instrumen. and Meas. Vol. 64, No. 6, pp. 1716 - 1725, 2015.
10. Y. Le Sage, M. Charles, J. -M. Lerat, "Measurement of antenna parameters under a controlled temperature," 17<sup>th</sup> International Congress of Metrology, Paris, France, Aug. 2015. doi: 10.1051/metrology/201512010
11. S. S. Dash, F. Pythoud, P. Leuchtman and J. Leuthold, "Traceable Power Measurement of LTE Signals," 17<sup>th</sup> International Congress of Metrology, Paris, France, Aug. 2015. doi:10.1051/metrology/20152005.
12. S. S. Dash, F. Pythoud, M. Hudlicka, "RF Power Metrology in LTE Systems" (original title in Czech: "Měření výkonové úrovně v LTE systémech"), 43<sup>rd</sup> meeting of the Czech electrotechnical society, subgroup Microwave tech., Prague, 18<sup>th</sup> Nov. 2015, pp. 1-4.
13. D. McCormick, "Femtosecond Lasers Drive a New Generation of Network Vector Analyzers," IEEE Spectrum, 16th Nov. 2015. Available at <http://spectrum.ieee.org/tech-talk/at-work/test-and-measurement/femtosecond-lasers-drive-a-new-generation-of-network-vector-analyzers>
14. M. Bieler, H. Fuser, K. Pierz, "Time-Domain Optoelectronic Vector Network Analysis on Coplanar Waveguides," IEEE Transactions on Microwave Theory and Techniques, vol. 63, no. 11, pp. 3775–3784, Nov. 2015.

15. A. Visweswaran; C. de Martino; E. Sirignano; M. Spirito, "An IQ-steering technique for amplitude and phase control of mm-wave signals," Microwave Measurement Conference, 2015 86<sup>th</sup> ARFTG, Atlanta, GA, 2015, pp. 1-4.
16. L. Le Coq, B. Fuchs, T. Kozan, S. Burgos and P. O. Iversen, "IETR millimeter-wave Compact Antenna Test Range implementation and validation," 2015 9<sup>th</sup> European Conference on Antennas and Propagation (EuCAP), Lisbon, 2015, pp. 1-5.
17. D. A. Humphreys, A. Raffo, G. Bosi, G. Vannini, D. Schreurs, K. N. Gebremicael and K. Morris, "Maximizing the Benefit of Existing Equipment for Nonlinear and Communication Measurements," 87<sup>th</sup> ARFTG Microwave Meas. Conf. Interactive Forum, ISBN: 978-1-5090-1308-1
18. M. Hudlicka, C. Lundström, D. A. Humphreys, I. Fatadin, "BER estimation from EVM for QPSK and 16-QAM coherent optical systems," International Conference on Photonics (ICP), Kuching, 2016, pp. 1-3.
19. Soumya Dash and Frederic Pythoud, "A reference setup to calibrate LTE Code selective field probes," METinfo, vol. 23 no. 1, 2016. Available at: <https://www.metas.ch/dam/data/metas/Dokumentation/METASPublikationen/metinfo/METinfo/2016/A%20reference%20setup%20to%20calibrate.pdf>
20. S. Dash et al., "Approaching the shannon limit through constellation modulation," 2016 Optical Fiber Communications Conference and Exhibition (OFC), Anaheim, CA, 2016, pp. 1-3, Mar. 2016. doi:10.1364/OFC.2016.Th2A.46
21. T. H. Loh, C. Li, H. Wang and F. Qin, "A Software-Defined-Radio Platform for Multiple-Input-Multiple-Output Over-The-Air Measurement", Invited paper, the 10th European Conference on Antennas and Propagation (EuCAP 2016), Davos, Switzerland, 11th – 15th Apr. 2016.
22. C. Li, T.-H. Loh, D. A. Humphreys, Y. Gui, H. Wang and F. Qin, "A LTE MIMO OTA Test System Using Vector Signal Transceivers", the 25<sup>th</sup> European Conference on Networks and Communications (EuCNC 2016) on 14th Apr. 2016.
23. M. Alonso-del Pino, M. di Rosa, M. Simeoni, M. Spella and M. Spirito, "A Planar Near Field Setup for Millimeter-Wave System-Embedded Antenna Testing," in IEEE Antennas and Wireless Propagation Letters , vol. 16, no.99, pp.83 - 86., 21 Apr. 2016. doi: 10.1109/LAWP.2016.2557239
24. B. Fuchs, L. Le Coq and M. D. Migliore, "Fast Antenna Array Diagnosis from a Small Number of Far-Field Measurements," in IEEE Trans. Antenna. Propag., vol. 64, no. 6, pp. 2227-2235, June 2016".